Heuristic battery-protective strategy for energy management of an interactive renewables–buildings–vehicles energy sharing network with high energy flexibility

Energy Conversion and Management 214 (2020) 112891

Contents lists available at ScienceDirect

Energy Conversion and Management

journal homepage: www.elsevier.com/locate/enconman

Heuristic battery-protective strategy for energy management of an interactive renewables–buildings–vehicles energy sharing network with high energy flexibility

Yuekuan Zhou[a], Sunliang Cao[a,*], Jan L.M. Hensen[b], Ala Hasan[c]

[a] Renewable Energy Research Group (RERG), Department of Building Services Engineering, Faculty of Construction and Environment, The Hong Kong Polytechnic University, Kowloon, Hong Kong, China
[b] Department of the Built Environment, Eindhoven University of Technology (TU/e), Netherlands
[c] Technical Research Centre of Finland - VTT, Finland

ARTICLE INFO

Keywords:
Interactive Energy Sharing Network
Energy Management System
Energy Flexibility
Battery Degradation
Battery-protective Strategy
Vehicles Fleet Integration

ABSTRACT

Interactive energy sharing networks with centralised coordinated energy management between buildings and vehicles can increase eco-economics viability, while tracking battery degradations is critical to the assessment of techno-economic performance and energy flexibility. In this study, a mathematical model was developed to characterise the cycling aging of electrochemical battery storage in multidirectional interactions within interactive renewables–buildings–vehicles energy sharing networks, with classification of the cycle life into two groups (slow degradation zone and acceleration zone). An advanced battery-protective energy control strategy was developed that fully utilises inherent battery depreciation characteristics for flexible energy management. Multi-criteria were investigated, including equivalent CO_2 emissions, import cost, energy flexibility, and the equivalent relative capacity of battery storage. With respect to the advanced battery-protective energy control strategy, the grid-battery charging process can decrease the depth of discharge and thus slow down the battery depreciation rate, but it will also lead to an increase in the number of cycles along with cycling aging. The research results show that, in terms of cycling aging, the single-variable mathematical fitting method with piecewise fitting curves (correlation coefficient of 0.9807) is more accurate than the bivariate mathematical fitting method (correlation coefficient of 0.9206). In addition, the proposed battery-protective control strategy can contribute to multi-criteria improvement. Furthermore, robust solutions for relative capacity improvement have been proposed with a lower limitation of fractional state of charge at 0.7. This study formulated a synergistic interactive energy framework for flexible district energy management, involving complementary solar-wind renewable systems, static and mobile battery storage, diversified energy demands in district buildings, and an advanced battery-protective energy management strategy, which can provide technical guidance to designers, operators, and stakeholders in terms of flexible participation in smart and resilient district energy networks.

1. Introduction

1.1. Background

The deteriorating environment, increasing energy demand, and intensified energy shortages call for the necessary deployment of clean power production, advanced energy storage, energy-efficient systems, advanced energy management, and control strategies. Buildings and transportation account for considerable amounts of total energy consumption. For instance, in Hong Kong, buildings and transportation account for more than 90% of total energy consumption [1]. The formulation of flexible energy systems, such as interactive buildings–-vehicles–buildings energy sharing networks, is also an effective solution with respect to the intensified crisis of energy shortage and environmental issues. Synergistic functions between buildings and vehicles are good solutions for enhancing the resilience and flexibility of electric grids with fluctuations in the energy supply of multi-energy systems. Furthermore, flexible energy demand [2 3], diversified energy storage [4], and robust control strategies for energy management [5-9] are promising sources of flexibility for the utility grid.

With respect to energy storage, electric storage is more challenging and promising than thermal energy storage due to the higher energy

* Corresponding author.
E-mail addresses: sunliang.cao@polyu.edu.hk, caosunliang@msn.com (S. Cao).

https://doi.org/10.1016/j.enconman.2020.112891
Received 28 December 2019; Received in revised form 12 March 2020; Accepted 21 April 2020

Nomenclature

Symbols

E	energy [kWh]
ED	electric demand [kWh]
end	ending of the entire simulation process
G	renewable electricity generation [kWh]
P	power [kW]
t	time [h]

Greek

η	efficiency
τ	time-duration step [h]

Subscripts

eg	Electricity grid
exp	export
gen	generation
imp	import from the electricity grid
off-peak	off-peak period
peak	peak period
surp,REe	surplus renewable electricity
toSB,REe	renewable electricity to static battery
toEV,REe	renewable electricity to electric vehicles
toShutBus,REe	renewable electricity to shuttle buses
toSB,grid	grid electricity to static battery
toEV,grid	grid electricity to electric vehicles
toShutBus,grid	grid electricity to shuttle buses

Acronyms

AHU	air handling unit
BIPVs	building integrated photovoltaics
DHW	domestic hot water
Cap	storage capacity
CEF	CO_2 emission factor
DOD	depth of discharge
ECE	equivalent CO_2 emission
EV	electric vehicle
FSOC	fractional state of charge
GSR	off-peak grid shifted ratio
G2B	grid-to-battery
IC	import cost
RSR	off-peak surplus renewable shifted ratio
REe	renewable electricity
RC	relative capacity
SB	static battery
V2X	Vehicle-to-Grid/Building/Home

quality of electricity compared with that of thermal energy. Electric storage systems include electrochemical energy storage, compressed air storage, supercapacitor storage, and pumped storage. Because of advancements in technology and techno-economic competitiveness, electrochemical energy storage has been widely accepted in the market, e.g., lead-acid and lithium-ion batteries. Battery depreciation in the interactive renewables–buildings–vehicles energy sharing network is one of the most critical factors affecting renewable energy penetration, the shifting capability of off-peak grid electricity, the coverage of building demand, and the ramp rate of the power grid. In academia, studies on battery depreciation under a hierarchical control strategy of an interactive buildings–vehicles–buildings energy sharing network are quite rare. The formulation of an advanced energy control strategy to decelerate battery depreciation rate is highly desirable for system performance enhancement.

1.2. Literature review

The deployment of renewable systems can promote eco-economic performance, whereas the grid has to suffer from frequent import/export pressure, resulting from dynamically balancing renewable energy and energy demands as a virtual energy storage. Solutions for the energy flexibility enhancement include the Predictive rule-based control [10], controlled loads through multi-agent reinforcement learning [11] and model predictive control [12], thermal mass storage [13], and so on. Energy sharing between multi-energy systems is an effective solution to improve aggregated energy flexibility [14-16] provided by buildings to the utility grid. Synergy between buildings can improve the self-consumption and self-sufficiency ratios to 42% and 64%, respectively [15]. The retired EV battery storage [17] and the integration of various vehicles as energy carriers into multi-energy systems [18] of different high-rise buildings can expand the energy boundary from isolated single buildings to renewables–buildings–vehicles, which can increase renewable energy penetration [19], improve the reliability and robustness of demand coverage [19], decrease reliance on the grid [20], and improve resilience to the fluctuating energy supply of the grid. Several researchers have focused on the formulation and energy interaction mechanisms of interactive energy sharing networks. A collaborative energy interaction model was developed by Quddus et al. [21], including charging stations, commercial building clusters, and a power grid. The proposed technique was useful in guiding decision-makers on the development of interactive multi-energy systems. Cao [22] investigated the impact of boundary expansions on zero-emission office buildings. Research results indicated that the boundary expansion can enhance matching capabilities, building–vehicle energy interactions, and the renewable coverage of EV storage. Flores et al. [23] indicated that building-to-vehicle energy interaction can simultaneously reduce energy consumption and total operational costs. Barone et al. [24] investigated the techno-economic performances of a building-to-vehicle-to-building system with electric vehicles (EVs) as electric energy carriers. Their results indicated that the formulated building-to-vehicle-to-building system was promising in terms of decreasing grid reliance, reducing grid electricity consumption, and enhancing energy-matching indexes. Zhou et al. [25] provided a state-of-the-art literature review on energy interactions among different types of buildings and multi-diversified energy-fuelled vehicles. Several technical challenges were identified and clarified, including vehicle depreciation and power fluctuation of grids [25]. It is noteworthy that, as critical components in multi-energy systems, vehicle batteries suffer from accelerated depreciation rates when being integrated into building energy systems due to frequent charging/discharging cycles. Studies are quite limited on the dynamic characterization of battery performance in multidirectional energy interactions, such as in buildings-to-vehicles, vehicles-to-buildings, grid-to-buildings, buildings-to-grid, and grid-to-vehicles.

In academia, battery degradation in building energy systems has increasingly attracted researchers' interests. Tang et al. [26] experimentally tested Lithium-ion battery depreciation, with respect to different temperatures and aging levels. The results indicated that the voltage prediction error could be controlled within ± 20 mV. Ahmadian et al. [27] proposed a state-of-the art review on battery degradation, including calendar aging and cycling aging. The review can promote the development of smart grids through vehicle-to-grid (V2G) interactions. With the implementation of a genetic algorithm, Yang et al. [28] proposed a novel method to dynamically predict the

performance of lithium-ion batteries. Research results indicated that the proposed method was accurate with the maximum capacity and state-of-charge errors lower than 5.0% and 2.1%, respectively. Liu et al. [29] proposed a battery charging management strategy for techno-economic performance improvement. Thompson et al. [30] conducted a systematic literature review on the economic feasibility of Li-ion battery degradation in a vehicle-to-(grid/building/home) (V2X) system. According to their results, degradation mechanisms can be classified as calendar aging and cycling aging behaviours. Uddin et al. [31] indicated that there is no economic benefit when considering battery degradation. Salpakari et al. [32] developed an optimal control model following the characteristic of battery degradation to enhance the flexibility of a buildings–vehicles system. According to their results, due to increased battery degradation, the cost savings through V2G interactions are minor. It is noteworthy that the economic feasibility for integrating batteries in building energy systems is questionable when considering the cost of battery depreciation.

The PV–battery–vehicles system and energy management are promising to improve techno-economic performance [33,34] and mitigate reliance on micro-grids [35]. Mehrjerdia et al. [33] studied the system performance of a net-zero energy building with hybrid renewable energies and hydrogen storage. The cogeneration of hydro-solar systems can reduce CO_2 by approximately 39546 kg and the total cost by approximately 50.3%. Akhtari et al. [34] proposed an excess electricity recovery strategy. Their results indicated that the extra electricity recovery could improve the renewable fraction by up to 35% and reduce the cost of energy and CO_2 emission by 7.1% and 10.6%, respectively. When considering the recycling of the battery systems of retired vehicles for building energy storage, Assunção et al. [35] studied the techno-economic feasibility of a retired EV battery for residential PV energy storage. Salpakari et al. [32] developed an optimal control model to improve the techno-economic performances of net-zero energy houses and plug-in EV systems, considering thermal dynamics and battery degradation. The results indicated that due to increased battery degradation, the cost savings from vehicle-to-grid is minor compared to those of smart charging, even though the self-sufficiency can be increased. According to their results, for the 10th year of operation, the grid exportation was reduced from 82.1% to 79.7% for a large Nissan Leaf battery and from 78.8% to 69.9% for a small Citroen C0 battery. It is noteworthy that there are few studies on advanced control strategies for battery performance enhancement in multidirectional energy interactions with comprehensive considerations of renewable energy management, time-of-use grid electricity, the management of battery charging/discharging (i.e., depth of discharge and charging power), and the dynamic resilience of the grid.

Due to the sophisticated power flows in grid-connected renewables–buildings–vehicles energy sharing networks, the roles of renewable systems, hybrid batteries, and grids are complicated and dynamically case-dependent. Power flowing into battery systems can be either from renewable energy to improve renewable penetration [36] or from off-peak grid electricity for shifting capability enhancement [37]. The battery can contribute to a more flattened demand profile, with a peak shaving and valley-filling strategy, and contribute to the mitigation of reliance on micro-grids. Likewise, in addition to dynamically balancing real-time energy demands, the grid can improve the reliability of the battery for demand coverage with an improved storage capacity. However, the synergistic function between micro-grid and battery requires flexible operation of the charging power and the state of the charge of batteries. Otherwise, techno-economic performances are not desirable due to the energy-related contradiction: the grid-battery charging process can improve the depth of discharge, which slows down the battery depreciation rate, whereas the grid-battery charging process will lead to an increase in the number of cycles together with battery degradation. Therefore, systematic and parametric studies are necessary.

1.3. Scientific gaps and contributions of this paper

Generally speaking, three scientific gaps can be noted: 1) empirical formulas with constant coefficients in academia [30] for dynamic cycling aging are not feasible during frequent charging/discharging cycles of electrochemical battery storage in interactive buildings–vehicles systems; 2) energy management strategies in academia for grid-connected buildings and vehicle energy systems fail to systematically consider battery depreciation, renewable energy management, time-of-use grid electricity, management of battery charging/discharging (i.e., depth of discharge and charging power), and the dynamic resilience of micro-grids; and 3) the grid-responsive charging strategy proposed in academia [37] fails to consider the cycling aging characteristic in terms of the depth of discharge and the number of cycles. The energy contradiction through the synergistic function between renewable systems and the micro-grid for the improvement of battery relative capacity has not been effectively addressed. To be more specific:

1) In academia, studies on the dynamic characterization of cycling aging of electrochemical battery storage are quite limited, and existing methodology is normally based on empirical formulas with constant coefficients [30]. However, dynamic cycling aging is quite complicated, and coefficients in empirical formulas are dependent on depth-of-discharge and number of cycles during the processes of multidirectional energy interactions, such as buildings-to-vehicles, vehicles-to-buildings, grid-to-buildings, buildings-to-grid, grid-to-vehicles, and between vehicles. Therefore, empirical formulas with constant coefficients are not feasible for interactive buildings and vehicle systems.
2) For the enhancement of renewable penetration and mitigation of the grid reliance of grid-connected buildings and vehicle energy systems, multi-criteria performances are involved, including equivalent CO_2 emission, import cost, system energy flexibility, and equivalent relative battery capacity. There have been few studies on the development of advanced control strategies systematically considering the cycling aging of electrochemical battery storage, renewable energy management, time-of-use grid electricity, management of battery charging/discharging processes (i.e., depth of discharge and charging power), and the dynamic resilience of micro-grids.
3) With regard to the synergistic function between renewable systems and the micro-grid for the improvement of battery relative capacity, an energy contradiction can be noted: the grid-battery charging process can decrease the depth of discharge and thus slow down the cycling aging rate, whereas the grid-battery charging process will lead to an increase in the number of cycles together with battery degradation. However, this contradiction has been rarely discussed and effectively addressed in current academia.

The above-mentioned scientific gaps were addressed in this study. An interactive renewables–buildings–vehicles energy sharing network was formulated, systematically integrating hybrid renewable energy sources, diversified thermal and electric energy storage systems, and multidirectional power exchanges within buildings, vehicles, and grids. A mathematical model was developed and implemented in the renewables–buildings–vehicles system to characterise real-time battery degradation during the process of multidirectional interaction. An advanced battery-protective energy control strategy was proposed and implemented in an interactive renewables–buildings–vehicles energy sharing network for building energy management by fully utilising the inherent battery depreciation characteristics (i.e., renewable-battery and grid-battery charging in a slow degradation zone and the avoidance of grid-battery charging in an acceleration zone), the time-of-use grid electricity, and the management of battery discharging for energy shifting. With respect to battery charging and energy management in the interactive renewables–buildings–vehicles energy sharing network, the above-mentioned energy contradictions, as listed in item 3, are

presented and discussed together with effective technical solutions.

The novelty and contributions of this study are as follows:

1) A dynamic mathematical model was developed to characterise the cycling aging of electrochemical battery storage in multidirectional interactions within interactive renewables–buildings–vehicles energy sharing networks, with classification of the cycle life into two groups (slow degradation zone and acceleration zone). Compared to empirical formulas with constant coefficients, the proposed single-variable mathematical fitting method with piecewise fitting curves is more flexible for the dynamic transition of coefficients on empirical formulas, in accordance with the depth-of-discharge and number of cycles.
2) Based on the inherent cycling aging characteristics, an advanced battery-protective energy control strategy was proposed to improve the relative battery capacity, i.e., the renewable-battery and grid-battery charging in the slow degradation zone and the avoidance of grid-battery charging in the acceleration zone. Furthermore, the proposed battery-protective energy control strategy can improve techno-economic performance through the shifting of the off-peak grid electricity to the peak period and the management of depth of discharge and charging power for the battery discharging.
3) In terms of the contradiction of the grid-battery charging process (i.e., the grid-battery charging can decrease the depth of discharge and thus slow down the cycling aging rate, whereas the grid-battery charging process will lead to an increase in the number of cycles together with battery degradation), trade-off solutions have been proposed through comprehensive and systematic parametric analysis. The proposed solution can provide effective technical guidance to designers, operators, and stakeholders of multi-criteria performance improvement.

The remainder of this paper is organised as follows: the system is briefly described and demonstrated in Section 2; specifically, the building energy system, vehicle energy system, hybrid storage, and energy interactions are described. The system configuration and energy control strategy of the formulated interactive energy sharing network are presented, together with a reference case for comparative analysis purposes. In Section 3, both the mathematical model of battery depreciation and multi-criteria for the system assessment are described. Results and discussion are presented in Section 4. Conclusions are summarised in Section 5.

2. System description—building energy systems, vehicles, hybrid storage systems, and multidirectional energy interactions

2.1. Meteorological parameters

Meteorological parameters are presented in Fig. 1 [38]. The annual average ambient temperature in Hong Kong is 23 °C, while the ambient temperature is between 15 and 34.6 °C for approximately 91% of the year. The cooling and heating degree days (base temperature of 18 °C) are 2025 and 247, respectively [38]. The monthly average wind speed is between 3.6 and 5.7 m/s, together with a monthly solar radiation between 63.6 and 168 kWh/m^2.a.

2.2. HVACs, internal gains, and energy storage in high-rise offices and hotel buildings

In this study, two high-rise buildings were investigated: 30-floor office building and 30-floor hotel building. The geometrical parameters for each floor were 400 m^2 (20 m × 20 m) net floor area and 3.2 m height. Specifications of the cooling systems for both buildings are listed in Table 1, and the rated capacities of AHU cooling chillers for the office and hotel were 293 kW (Carrier 30RB302 [39]) and 93.9 kW (CGAD090 [40]), respectively. The rated capacities of space cooling chillers for the office and hotel were 506 kW (Carrier 30RB522 [39]) and 293 kW (Carrier 30RB302 [39]), respectively. The flow rates of fresh air were 8 L/s/person for the office building and 15 L/s/person for the hotel building, as in the Performance-based Building Energy Code [41]. The set-point temperature of the hot water supply was 55 °C.

Table 2 lists the design parameters of the storage systems. Static batteries were designed in each building for two purposes: dynamically balancing the energy demands and shifting the renewable and grid electricity from off-peak to peak periods.

2.3. Energy systems of vehicles

There were three groups of EVs (10 vehicles in each group) and three groups of public shuttle buses (three buses in each group) employed for this study. The battery storage capacity was 24 kWh for each EV [44] and 46 kWh for each public shuttle bus [45]. Table 3 lists detailed information for all vehicles in the vehicle fleets according to the available commercial products on the market.

2.4. Basic demand of the hybrid buildings–vehicles system

The duration curves of the energy demand in the interactive renewables–buildings–vehicles energy sharing network are shown in Fig. 2. Due to domestic heating usage, such as showers, the domestic hot water (DHW) heating demand in the hotel was much higher than that in the office. Furthermore, the peak power of the electric vehicle fleets was 96.3 kW. As shown in Fig. 3(a), the annual basic electricity demands of the high-rise office building and high-rise hotel building were 145.4 kWh/m^2.a and 135 kWh/m^2.a, respectively. As shown in Fig. 3(b), the peak powers of space cooling, AHU cooling, and total electricity demand were 599.6, 358.6, and 428.8 kW for the office building, respectively, and 301.6, 95.6, and 408.6 kW for the hotel building, respectively.

2.5. Hybrid wind-solar renewable system

In this study, a hybrid wind-solar complementary system was designed to address energy demands of buildings and vehicles. Building integrated photovoltaics (BIPVs) were integrated with vertical building façades to shade the solar radiation and to generate renewable energy. The total area of BIPVs for each building was 6140 m^2. The normalised power–wind speed curve was referenced from a typical commercial product [48]. The power-wind speed curve of the wind turbine is shown in Table 4. The wind turbine was installed off-site, as with off-shore wind turbine systems. Table 4 lists detailed parameters of renewable systems, i.e., wind turbine, BIPVs, and solar thermal collectors. It should be noted that the impact of performance degradation on renewable generation has not been considered. This was because for a one-year operation in this study, the system performance was more subjected to battery degradation than the renewable systems.

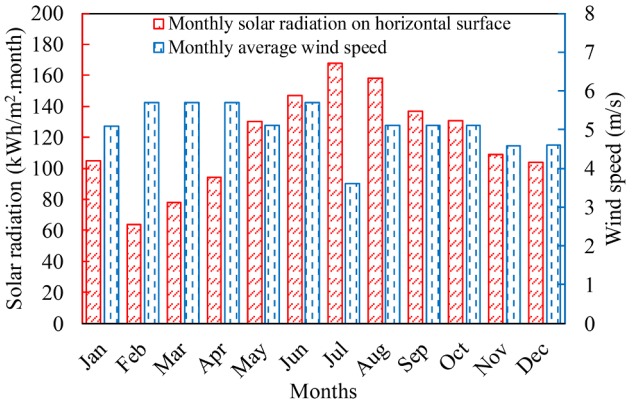

Fig. 1. Monthly wind velocity and monthly solar radiation in Hong Kong [38].

Table 1
Parameters of chillers in hotel and office buildings.

	High-rise hotel		High-rise office	
	Space cooling chiller	AHU cooling chiller	Space cooling chiller	AHU cooling chiller
Commercial product	Carrier 30RB302 [39]	CGAD090 [40]	Carrier 30RB522 [39]	Carrier 30RB302 [39]
Nominal COP	2.8	3.2	2.6	2.8
Rated capacity	293 kW	93.9 kW	506 kW	293 kW
Set-point temperature	15 ˚C	7 ˚C	15 ˚C	7 ˚C
Type in the TRNSYS	Type 655 [42]			

Table 2
Parameters of thermal and electric storage systems for the reference design.

Energy system	Building	Storage	Storage capacity	Thermal loss coefficient	Type in the TRNSYS
Thermal system	High-rise office building	AHU cooling tank	25 m^3	0.3 W/(m^2 K)	Type 534 [43]
		Space cooling tank	15 m^3		
		DHW tank	0.45 m^3		
	High-rise hotel building	AHU cooling tank	25 m^3		
		Space cooling tank	15 m^3		
		DHW tank	4.5 m^3		
Electric system	High-rise office building	Battery	300 kWh		Self-developed model
	High-rise hotel building	Battery	300 kWh		

Table 3
Energy system of vehicles in each group.

	Commercial product	Battery capacity (kWh)	Daily travelling distance (km/day)	Electricity consumption (kWh/km)
EV Group 1	Private electric vehicle/NISSAN LEAF [44]	24 [44]	45.5	0.15 [44]
EV Group 2			35.5	
EV Group 3			25.5	
Mini-bus in each group	Autonomous mini-bus/ST Autobus (RD 3154 K) [45]	46 [45]	31.2	1.2 [45]

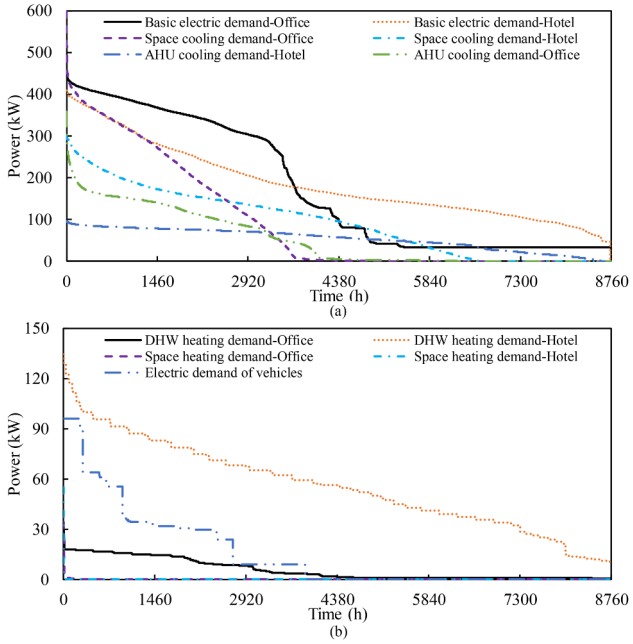

Fig. 2. Duration curves of demand for the renewables–buildings–vehicles system: (a) cooling and electrical demands and (b) heating and transportation demands.

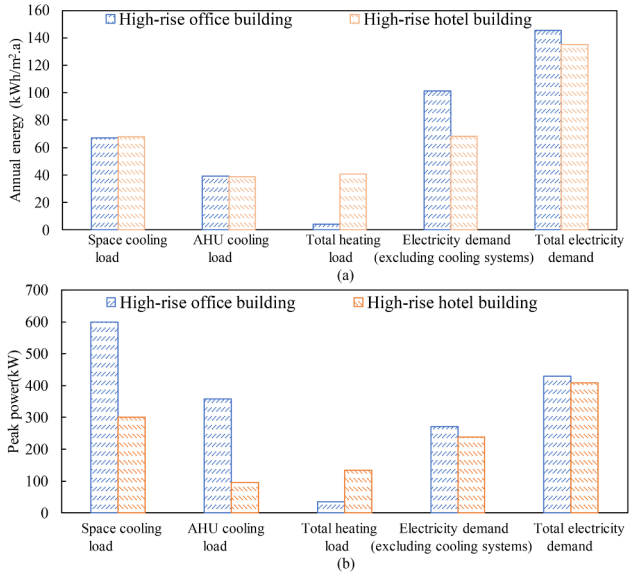

Fig. 3. Energy demands and peak powers. (Note: the total heat load included the hydronic AHU and DHW heating load. Electricity demand included lighting, equipment, ventilation fans, and pumps).

2.6. Local electric grid information

An off-peak and peak time-of-use electricity tariff was available for the economic assessment, as shown in Table 5 [49]. No grid feed-in tariff was considered. The 'off-peak period' was 21:00 PM-09:00 AM for working days, and 24/7 for holidays. The 'peak period' was 09:00 AM-21:00PM for working days.

Table 4
Parameters of the renewable systems.

	Parameters	Value
Wind turbine (off-site)	Type in TRNSYS 18	90 [47]
	Type of the wind turbine	3-blade [48]
	Hub height (m)	50
	Rated power (MW)	Case dependent
	Rotor diameter (m)	54
	Rated wind speed (m/s)	10
	Cut-in/cut-out wind speed (m/s)	3.5/25
	Site shear exponent	0.22
BIPVs	Type in TRNSYS 18	567 [46]
	Reference PV efficiency	0.1427
	Reference temperature	25
	Reference radiation (W/m^2)	1000
	Absorptance of the PV surface for solar radiation	0.9
	Extinction coefficient (m^{-1})	4
	Cover emissivity	0.9
	Channel emissivity - bottom	0.9
	Channel emissivity - top	0.09
	Efficiency modifier - radiation (m^2/W)	0.00009
	Cover thickness	0.00635
	Cover conductivity	5.04
	Efficiency modifier - temperature	−0.005
	Channel height	0.0508
	Refractive index	1.526
	Substrate resistance	0.422
	Back resistance	0.1204
Solar thermal collector	Type in TRNSYS 18	71 [47]
	Intercept efficiency	0.7
	Area of the evacuated solar thermal collector (m^2)	45
	Negative first-order efficiency coefficient (W/m^2K)	2.78
	Negative second order efficiency coefficient (W/m^2K^2)	0.008

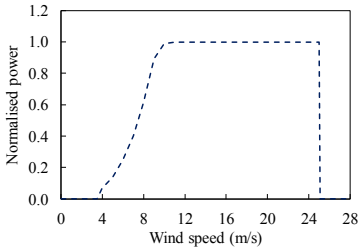

Table 5
Grid electricity cost for high-rise buildings in Hong Kong [49].

E_{imp} (each month, kWh)	$C_{grid,imp1}$ [a] (HK$/kWh)		$P_{peak,max}$ (each month, kVA)	$C_{grid,imp2}$ [b] (HK$/kVA)		Fuel surcharge cost, $C_{grid,imp3}$ [c] (HK$/kWh)
	Off-peak period	Peak period		Off-peak period[d]	Peak period[e]	0.278
< 200,000	0.649	0.726	≤ 650 kVA	0	68.4	
greater than200,000		0.71	greater than 650 kVA	26.8	65.4	

[a] '$C_{grid,imp1}$' is the energy charge price.
[b] '$C_{grid,imp2}$' is the demand charge price.
[c] '$C_{grid,imp3}$' is the fuel cost.

2.7. System configuration and control strategy

2.7.1. Systematic configuration of the interactive buildings–vehicles–buildings energy sharing network

The configuration of the formulated interactive renewables–buildings–vehicles energy sharing network is shown in Fig. 4, consisting of a wind-solar complementary system, static energy storage systems (hybrid heating/cooling storage systems and static batteries), EV system, and flexible multidirectional power interactions. It is noteworthy that within the renewables–buildings–vehicles energy sharing network, the vehicle systems were fully utilised with two purposes: 1) coverage of mobility consumption and 2) energy carriers between different buildings. In this sense, the vehicles as flexible mobility storage systems further improved the renewable penetration and reduced grid reliance. Note that in this study, off-site wind turbines were within the office and hotel building boundaries. The renewable energy from BIPVs and off-site wind turbines in the office building cannot be directly transferred to the hotel building, but it can be by the vehicle fleets for the energy sharing purpose. The electric grid is a virtual storage to dynamically balance the energy for each building through the grid's interactions.

2.7.2. Grid-responsive control strategy

The main difference between this study and our previous study [50] is that in our previous study [50], battery depreciation was not considered during charging/discharging processes, and the grid-responsive battery charging strategy was independent of the dynamic performance of battery systems [50]. In this study, the battery depreciation during charging/discharging processes was considered, and the grid-responsive battery charging strategy was dependent on the dynamic performance of the batteries. The energy management of the formulated interactive renewables–buildings–vehicles energy sharing network is shown in Fig. 5. As shown in Fig. 5, in the grid-responsive control strategy, according to the grid information, as listed in Table 5, both the renewable generation and grid electricity were classified into peak and off-peak energy. Depending on the management of the power flow, the grid-responsive control strategy included the hierarchical control strategy and battery-protective control strategy.

With respect to the hierarchical control strategy, at the peak time, the building electricity demand was covered by renewable energy, then by electrical storage. The remaining electric demand was covered by the grid electricity. For the management of surplus renewable energy, it was used to charge vehicles and then static batteries, before being

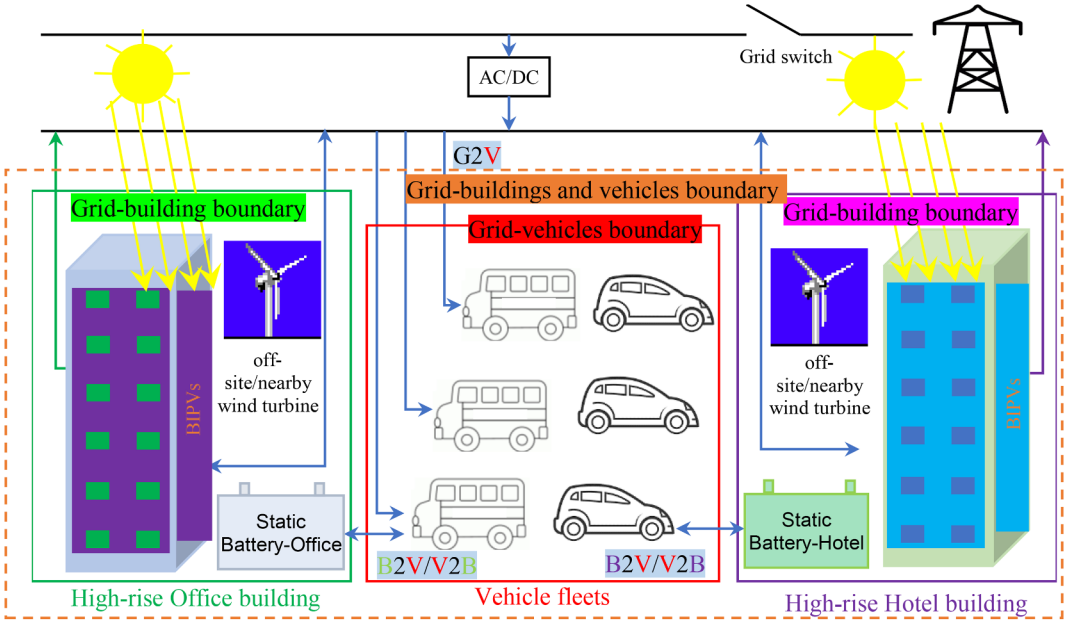

Fig. 4. Schematic diagram of the interactive renewables–buildings–vehicles energy sharing network. (Note: B2V and V2B indicate the building-to-vehicles and vehicles-to-building interactions, respectively. G2V indicates grid-to-vehicles interaction. The 'grid-building boundary' and 'grid-vehicles boundary' indicate boundaries of the conventional isolated system. The 'grid-buildings and vehicles boundary' indicates the boundary of the formulated interactive renewables–buildings–vehicles energy sharing network. The grid switch was on whenever there was grid importation and exportation and was off whenever there was no grid interaction.)

exported to the electricity grid. During the off-peak period, for the purpose of shifting the off-peak renewable energy/grid electricity to peak time, the hybrid electrical storage systems were charged by renewable energy and grid electricity for building usage at peak time.

Regarding the battery-protective control strategy, the energy management strategy was similar to the hierarchical control strategy during peak periods. The main difference was that at off-peak time, the battery charging strategy was dependent on the battery depreciation zones. For the purpose of energy shifting from off-peak to peak periods and the deceleration of battery depreciation rate, the hybrid electrical storage systems were charged by both renewable energy and grid electricity in the slow degradation zone, whereas the hybrid electrical storage systems were only charged by the surplus renewable energy in the acceleration zone.

The main difference between the hierarchical and battery-protective control strategy was that the off-peak grid-battery charging ($P_{off\text{-}peak,EVs}$, $P_{off\text{-}peak,Office}$, and $P_{off\text{-}peak,Hotel}$, as marked by dashed rectangles in Fig. 5) was only in the slow degradation zone in the battery-protective control strategy, whereas the off-peak grid-battery charging occurred during the entire off-peak period in the hierarchical control strategy. The slow degradation zone will be clearly shown in Section 3.1 as battery degradation modelling-determination of relative capacity.

Fig. 6 shows the power flow for the hierarchical and battery-protective control strategy. With respect to the simplified diagram, as shown in Fig. 6(a), during the peak period, to protect the vehicle battery, the first priority for discharging the battery is given to the static battery (as the vehicle battery is normally more expensive than the static battery). The first priority for charging the battery is given to the vehicle battery for the coverage of transportation demand and energy sharing. During the off-peak period, the hybrid electrical storage systems were charged by the off-peak grid electricity, which can be shifted to a peak period. The readers are highly recommended to refer to Fig. 6(b) for a more detailed description. As shown in Fig. 6(b), with respect to the hierarchical control strategy, at off-peak time, for the purpose of shifting the off-peak grid electricity to peak period, the hybrid electrical storage systems were charged by the off-peak grid electricity whenever the FSOC was lower than 0.9, as marked by the red and dashed diamonds in Fig. 6(b). Regarding the battery-protective control strategy, at off-peak time, the hybrid electrical storage systems were charged by the off-peak grid electricity when the FSOC was lower than 0.9 and the relative capacity was higher than 0.96, as marked by the red and dashed diamonds in Fig. 6(b). The reason for the avoidance of grid-battery charging in the battery-protective control strategy was that the battery depreciation rate was relatively fast when the relative capacity was lower than 0.96. In summary, the main difference between the hierarchical and battery-protective control strategy was that, as marked by the red and dashed diamonds, off-peak grid-battery charging only occurred when the relative capacity was higher than 0.96 in the battery-protective control strategy, whereas off-peak grid-battery charging was independent of the battery relative capacity in the hierarchical control strategy.

2.8. Reference case

In comparative energy studies, the reference case is the traditional control strategy according to the dynamic renewable-demand relationship for the energy management of formulated interactive renewables–buildings–vehicles energy sharing networks. Fig. 7 shows a schematic diagram and the energy flow of the reference case. When the renewable generation was higher than demand, the surplus energy was used to charge the vehicle batteries and then static batteries before being exported to the grid. In contrast, the shortage was covered by electricity from the static battery, then from vehicle batteries, and then imported from the grid.

3. Methodology

3.1. Battery degradation modelling-determination of the relative capacity

The mathematical model of battery degradation was developed according to the relative capacity performance of the commercial product RA12-200D [51]. The RA12-200D was an absorbent glass mat (AGM) deep-cycle battery designed for frequent cyclic discharge usage.

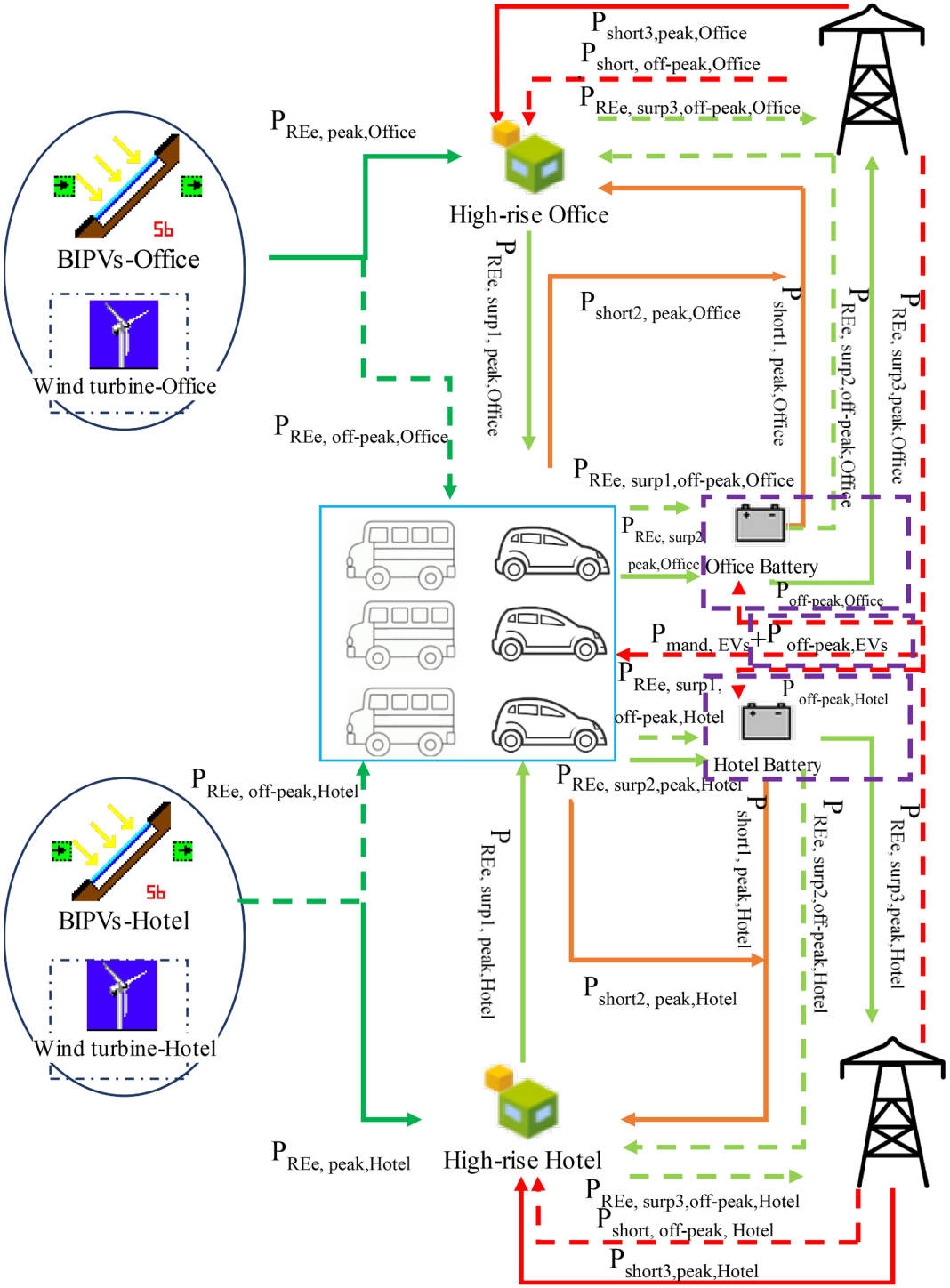

Fig. 5. Grid-responsive control strategy: hierarchical control strategy and battery-protective control strategy [50]. (Note: $P_{mand,EVs}$ and $P_{off\text{-}peak,EVs}$ denote the charging power of the vehicles in the mandatory mode and grid-to-battery charging during the off-peak period, respectively).

The AGM deep-cycle battery was specially designed for the vehicles system due to its high performance and enhanced electrical reliability [52].

Several factors may affect the length of cyclic service, including the depth of discharge (DOD), ambient temperature, and charging/discharge power [53]. It is noteworthy that the annual average ambient temperature is 23 °C in Hong Kong, while the ambient temperature varies between 15 and 34.6 °C for approximately 91% of the year (according to the duration curve in Fig. 1(a)). Correspondingly, according to [51], the battery capacity factors are marginally sensitive with respect to the aforementioned temperature range in Hong Kong. Therefore, in this study, the impact of the ambient temperature on dynamic battery depreciation was not considered. The most critical factors for the cycling aging, i.e., the depth of discharge and charging/discharge power, were considered, following the mathematical model, as shown in Fig. 8. As the materials used in the cathode and anode in the batteries suffered from oxidation and reduction reactions during charging and discharging cycles, the performance of the electrode materials depreciated with different magnitudes, which was the underlying mechanism of the capacity degradation of the battery. As

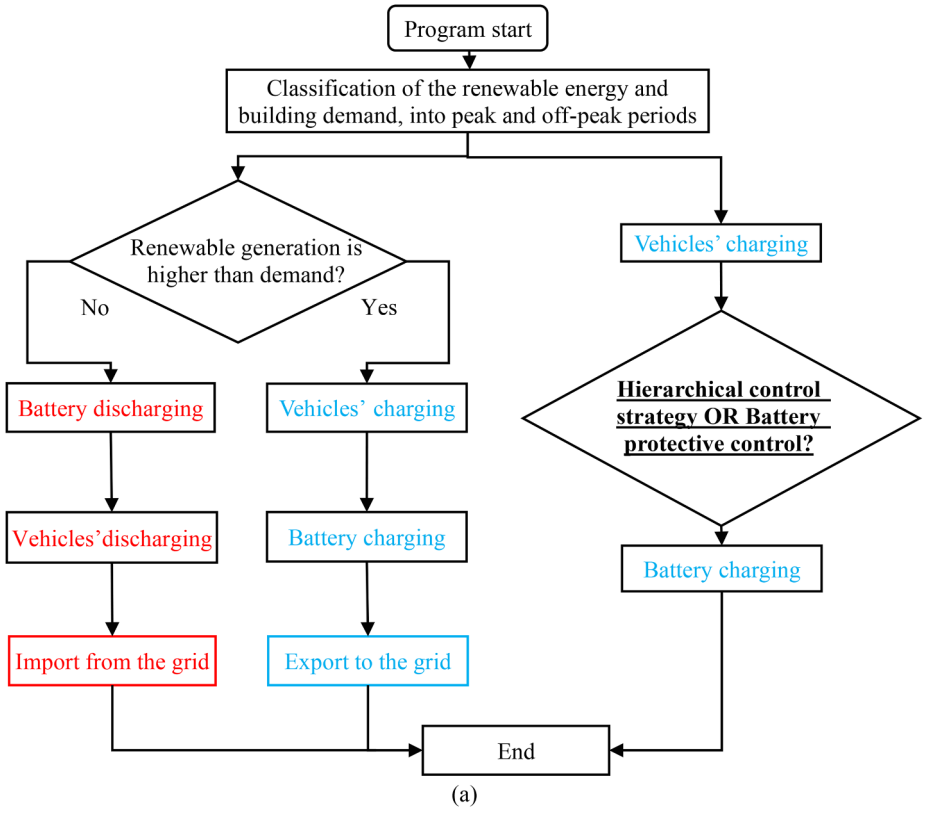

Fig. 6. Energy flow chart of the hierarchical control strategy and battery-protective control strategy: (a) a simplified diagram and (b) detailed energy flow chart with constraints. (Note: 'RC' is the abbreviation for the 'relative capacity'. 'SB' is the abbreviation for the 'static battery', which includes the batteries in the office and the hotel.)

shown in Fig. 8, there were two regions in the battery degradation curve, i.e., the slow degradation zone (early cycles) and acceleration zone. In the slow degradation zone, the depreciation rate was less sensitive to the number of cycles, as indicated by the slow curve slope. In the acceleration zone, the depreciation rate was sensitive to the number of cycles, and the decreasing magnitude of the relative capacity accelerated with the increasing number of cycles.

To quantitatively and accurately characterize the relative capacity with respect to the DOD and number of cycles, two lsqcurvefit (least square curve fitting) estimation-based fitting methodologies were adopted and compared, i.e., bivariate mathematical fitting method and single-variable mathematical fitting method with piecewise fitting curves. The fitting equation using the bivariate mathematical fitting method is shown in Equation (1). As shown in Equation (1), for regression using the bivariate mathematical fitting method, the two-way interaction of two variables was considered:

$$RC_{DoD,t+\tau} = \sum_{m=0}^{n} k_m x^{n-m} \cdot \sum_{m=0}^{n} k'_m y^{n-m} \quad (1)$$

where n is the exponential power (n = 1, 2, and 3), k_m and k'_m are coefficients, and x and y refer to the number of cycles and depth of discharge, respectively.

The DOD indicates how deeply the battery is discharged. The larger the DOD, the smaller the available number of cycles will be. In this study, the dynamic DOD was updated for each time step using Equation (2). Regarding the single-variable mathematical fitting method with piecewise fitting curves, as expressed in Equation (3), the fitting equations included the linear fitting equation in the slow degradation zone and the parabolic fitting equation in the acceleration zone. The underlying mechanism of the battery depreciation is demonstrated in Fig. 8(b). As a critical parameter, the lower fractional state of charge ($FSOC_{lower}$) refers to the low fractional state of charge during the charging/discharging processes. In other words, the grid charged the battery system whenever the fractional state of charge was lower than the $FSOC_{lower}$. The first step was to characterize the number of cycles of two DOD-based adjacent curves using the inverse function of the relative capacity function ($CycleNum_{DOD1,t}$ and $CycleNum_{DOD2,t}$, as shown in Fig. 8(b)) according to the dynamic DOD. Afterwards, the numbers of cycles in the follow-up time step ($CycleNum_{DOD1,t+\tau}$ and $CycleNum_{DOD2,t+\tau}$) were updated, as shown in Equations (4). Based on the updated $CycleNum_{DOD1,t+\tau}$ and $CycleNum_{DOD2,t+\tau}$, the relative capacity at the next time step $t_{+\tau}$ ($RC_{DOD1,t+\tau}$ and $RC_{DOD2,t+\tau}$) could be calculated using Equation (3). Thereafter, the relative capacity at the dynamic DOD ($RC_{DOD,t+\tau}$) could be calculated, following the linear interpolation, as shown in Equation (6).

$$DOD=1\text{-}FSOC_{valley,cycle\ n} \quad (2)$$

where $FSOC_{valley,cycle\ n}$ is the lowest FSOC for the n^{th} cycle.

$$RC_{DOD}=\begin{cases} k_{1,DoD}\ x + k_{2,DoD} & \text{the slow degradation zone} \\ k'_{1,DoD}x^2 + k'_{2,DoD}\ x + k'_{3,DoD} & \text{the acceleration zone} \end{cases} \quad (3)$$

$$CycleNum_{t+\tau} = CycleNum_t + \Delta CycleNum_{t+\tau} \quad (4)$$

$$\Delta CycleNum_{t+\tau} = \frac{E_{battery,t\to t+\tau}}{Cap_{battery,ini} \times 2\times DoD} = \frac{|FSOC_{t+\tau}\text{-}FSOC_t\ | \times Cap_{battery,t}}{Cap_{battery,ini} \times 2\times DoD} \quad (5)$$

$$RC_{DoD,t+\tau} = \frac{DoD_{t+\tau}\text{-}DoD_2}{DoD_1\text{-}DoD_2} \times RC_{DoD1,t+\tau} + \frac{DoD_{t+\tau}\text{-}DoD_1}{DoD_1\text{-}DoD_2} \times RC_{DoD2,t+\tau} \quad (6)$$

where k and k' are coefficients of the fitting equation in the slow degradation zone and acceleration zone, respectively. The subscript, *i,DoD*, indicates the i^{th} coefficient of the curve at the DOD. *RC* is the

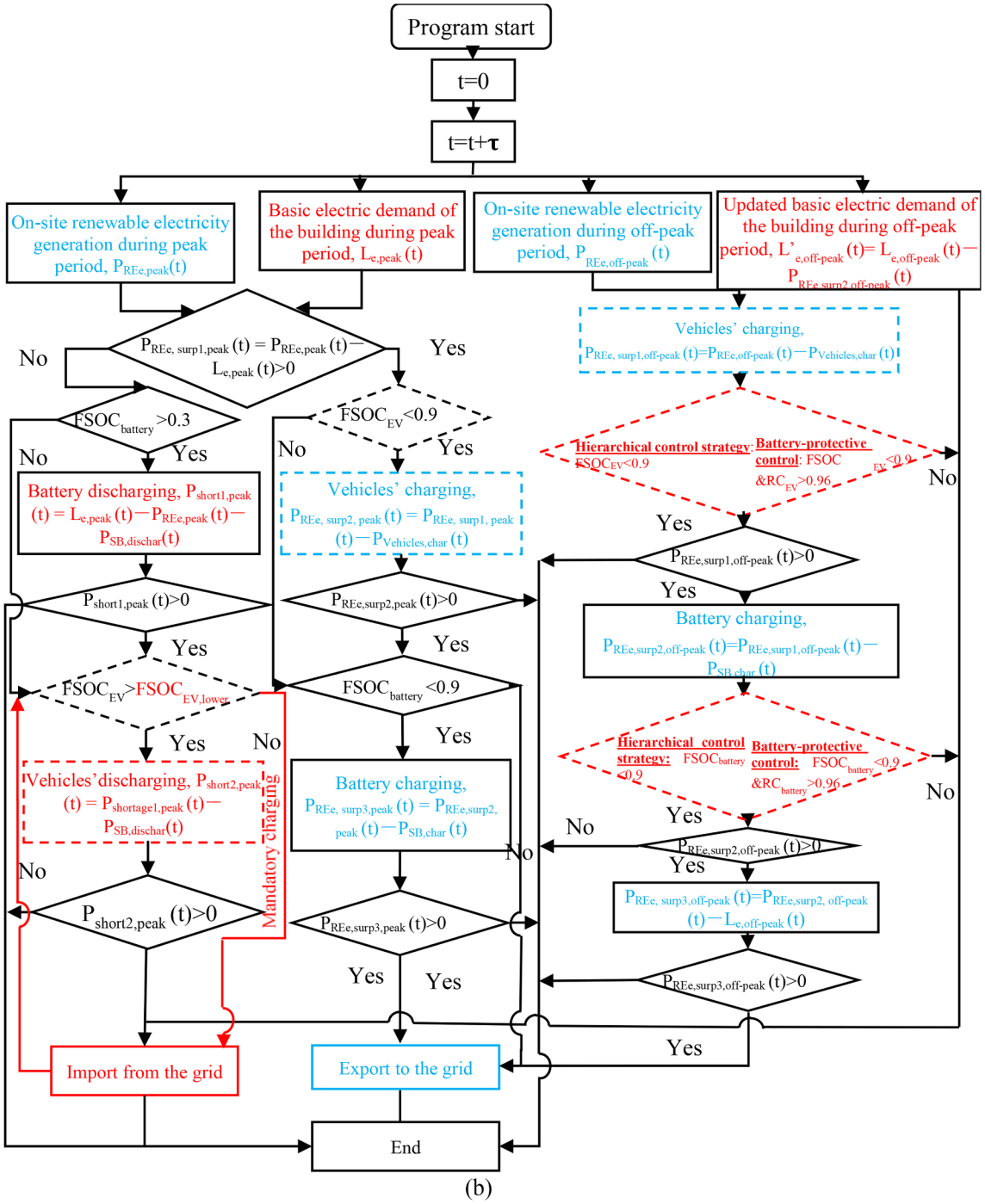

Fig. 6. (*continued*)

relative capacity. t and $t + \tau$ indicate the time at t and one-time step (τ) later. $Cap_{battery,ini}$ and $Cap_{battery,t}$ are battery storage capacities at the initial state and time t, respectively. $E_{battery,t\to t+\tau}$ is the net energy charging to or discharging from the battery for one time step.

The correlation results of the relative capacity are shown in Fig. 22, Appendix. As shown in Fig. 22, compared to the bivariate mathematical fitting method with the highest correlation of determination at 0.9206, the single-variable mathematical fitting method with piecewise fitting curves improved the correlation coefficient to 0.9807. Thereafter, the single-variable mathematical fitting method was adopted to develop the battery depreciation model.

The five statistical indicators were calculated to evaluate the prediction accuracy on the dynamic battery cycling aging, including the coefficient of determination (R^2), mean absolute error (MAE), root mean square error (RMSE), normalized mean bias error (NMBE), and coefficient of variation for the root mean-square error (CV-RMSE). As listed in Table 6, the single-variable mathematical fitting model with piecewise fitting curves is more robust than the bivariate mathematical fitting model with the R^2, MAE, RMSE, NMBE, and CV-RMSE at 0.981, 0.010, 0.018, 1.15%, and 2.01%, respectively. This indicates that the developed single-variable mathematical fitting model with piecewise fitting curves is accurate for the prediction of dynamic battery cycling aging.

3.2. Assessment criteria for the interactive energy sharing network—import cost, equivalent CO_2 emissions, and energy flexibility

In this study, multi-dimensional assessment criteria were involved with respect to different perspectives, including the energy flexibility

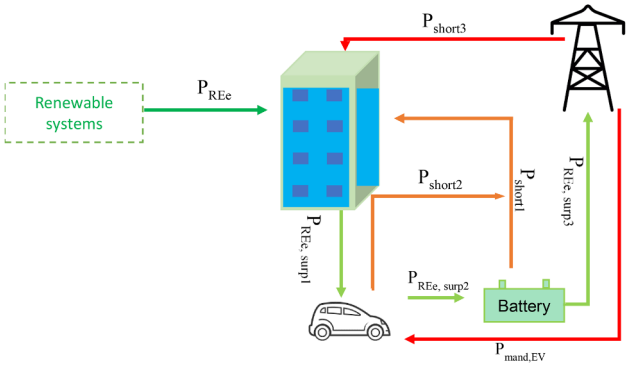

Fig. 7. Traditional control strategy of the renewables–buildings–vehicles energy system.

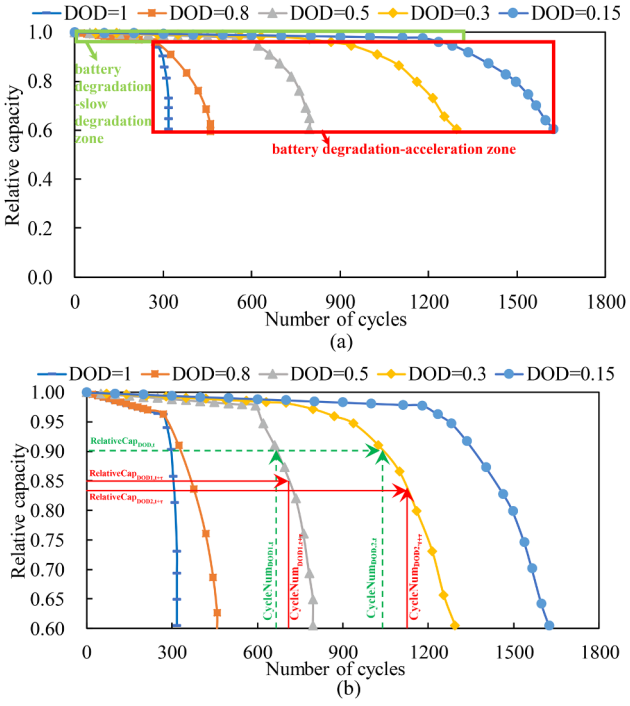

Fig. 8. (a) Evolution of the relative capacity of the battery with respect to DOD and number of cycles and (b) demonstration of the battery depreciation mechanism. (Note: the dashed green lines indicate the state at current time t, and the solid red lines indicate the state at the next time step t + τ).

performance (i.e., off-peak surplus renewable shifted ratio (RSR), and off-peak grid-shifted ratio (GSR)), economic performance (i.e., import cost of the buildings–vehicles system (IC)), and emission performance (i.e., annual net equivalent CO_2 emission (ECE)).

3.2.1. Energy flexibility

The off-peak surplus RSR is the ratio of renewable electricity stored during the off-peak period, $E_{off\text{-}peak,REe}$, to the total on-site surplus renewable electricity, $E_{surp,REe}$. The off-peak GSR is the ratio of grid electricity stored during the off-peak period, $E_{off\text{-}peak,grid}$, to the total amount of electricity imported from the grid, E_{imp} [37].

$$E_{off-peak,REe} = \int_0^{t_{off\text{-}peak}} [P_{toSB,REe}(t) + P_{toEV,REe}(t) + P_{toShutBus,REe}(t)]dt \quad (7)$$

$$E_{surp,REe} = \int_0^{t_{end}} P_{surp,REe}(t)dt \quad (8)$$

$$RSR = \frac{E_{off\text{-}peak,REe}}{E_{surp,REe}} \quad (9)$$

$$E_{off-peak,grid} = \int_0^{t_{off\text{-}peak}} [P_{toSB,grid}(t) + P_{toEV,grid}(t) + P_{toShutBus,grid}(t)]dt \quad (10)$$

$$E_{imp} = \int_0^{t_{end}} P_{imp}(t)dt \quad (11)$$

$$GSR = \frac{E_{off\text{-}peak,grid}}{E_{imp}} \quad (12)$$

3.2.2. Economic performance

To investigate the economic feasibility, the economic performance of the renewables–buildings–vehicles system was calculated as follows:

$$IC_1 = \int_{ti}^{te} P_{imp,office}(t)\cdot C_{eg,imp}(t)dt \quad (13)$$

$$IC_2 = \int_{ti}^{te} P_{imp,hotel}(t)\cdot C_{eg,imp}(t)dt \quad (14)$$

$$IC_{Vehicles} = \int_{ti}^{te} P_{imp,vehicles}(t)\cdot C_{eg,imp}(t)dt \quad (15)$$

$$IC = IC_1 + IC_2 + IC_{Vehicles} \quad (16)$$

where IC_1, IC_2, $IC_{Vehicles}$, and IC are import costs of the offices, hotel, vehicles, and buildings–vehicles system (HK$/m^2), respectively. $C_{eg,imp}$ is the import electricity price from the grid. $P_{imp,office}(t)$, $P_{imp,hotel}(t)$, and $P_{imp,vehicles}(t)$ are the instantaneous imported power from the grid in the offices, hotel, and vehicles (kW), respectively.

3.2.3. Annual net equivalent CO_2 emissions

The annual net equivalent CO_2 emissions of the renewables–buildings–vehicles system was calculated as follows:

$$ECE_1 = \int_{ti}^{te} [P_{imp,office}(t)\cdot CEF_{eg}(t) - P_{exp,office}(t)\cdot CEF_{eg}(t)]dt \quad (17)$$

$$ECE_2 = \int_{ti}^{te} [P_{imp,hotel}(t)\cdot CEF_{eg}(t) - P_{exp,hotel}(t)\cdot CEF_{eg}(t)]dt \quad (18)$$

$$ECE_{Vehicles} = \int_{ti}^{te} [P_{imp,vehicles}(t)\cdot CEF_{eg}(t)]dt \quad (19)$$

$$ECE = ECE_1 + ECE_2 + ECE_{Vehicles} \quad (20)$$

where $P_{exp,office}(t)$ and $P_{exp,hotel}(t)$ are the instantaneous exported power to the grid in the offices and hotel building (kW), respectively. The default value of CEF_{eg} is 0.7 kg $CO_{2,eq}$/kWh$_{end}$ [54]. ECE_1, ECE_2, and $ECE_{Vehicles}$ are equivalent CO_2 emissions of the offices, hotel buildings, and vehicles, (kg/m^2), respectively. ECE is the equivalent CO_2 emission of the integrated system (kg/m^2). Other variables are defined above.

Table 6
Cycling aging prediction errors between different models.

	R^2	MAE	RMSE	NMBE	CV-RMSE
Bivariate mathematical fitting model (power at 1)	0.598	0.058	0.075	6.26%	8.12%
Bivariate mathematical fitting model (power at 2)	0.828	0.036	0.050	3.94%	5.37%
Bivariate mathematical fitting model (power at 3)	0.921	0.025	0.034	2.65%	3.66%
Single-variable mathematical fitting model with piecewise fitting curves	0.981	0.010	0.018	1.15%	2.01%

3.2.4. Equivalent relative capacity

To characterise the dynamic performance of hybrid battery systems, the equivalent relative capacity ($RC_{total,end}$) of the battery was proposed and calculated by Equation (21):

$$RC_{total,end} = \sum_{i=1}^{8} \frac{Cap_{i,ini}}{Cap_{total,ini}} \times RC_{i,end} \quad (21)$$

where i refers to the i^{th} battery group. As there were a total of eight batteries (two static batteries in the offices and hotel, three battery groups of EVs, and three groups of public shuttle buses), the range of i was 1 to 8. $Cap_{i,ini}$ is initial storage capacity (without any depreciations) of the i^{th} battery group (such as the static battery in offices and hotel, batteries of electric vehicles within the three groups, and batteries of shuttle buses within the three groups). $Cap_{total,ini}$ is the accumulated storage capacity of the entire battery system.$RC_{i,end}$ is the relative capacity of the i^{th} battery group at the end of simulation.

4. Results and discussion

4.1. Comparison of system performance and battery depreciation between control strategies

4.1.1. Hierarchical charging mechanism with same settings of charging power and lower limitation of fractional state of charge ($FSOC_{lower}$)

With respect to the adoption of the formulated grid-battery charging process to protect the battery in this study, one critical contradiction must be noted, i.e., the grid-battery charging process could improve the depth of discharge and thus slow down the battery depreciation rate, whereas the grid-battery charging process leads to an increase in the number of cycles together with battery degradation. In this section, the technical feasibility of the grid-battery charging process was investigated through a comparative analysis with the reference case. A systematic and comprehensive parametric analysis was conducted to provide technical guidance to system managers with respect to the multi-criteria of the renewables–buildings–vehicles system.

Fig. 9 shows the annual electricity in hybrid battery systems. As shown in Fig. 9(a), compared to the traditional control strategy with the total annual electricity charged to vehicle batteries at 25.7 kWh/m^2.a, the total annual electricity charged to vehicle batteries in the hierarchical control and battery-protective control was much higher at approximately 35.3 kWh/m^2.a. This is due to the implementation of the grid-battery charging strategy to shift off-peak grid electricity to peak time, as introduced in Section 2.7.2 (Fig. 5). Overall, the total annual electricity charged to battery systems was 31, 37.1, and 37 kWh/m^2.a for the traditional, hierarchical, and battery-protective control strategy, respectively. The total annual electricity from batteries was 27.9, 33.4, and 33.3 kWh/m^2.a, as shown in Fig. 9(b), for the traditional, hierarchical, and battery-protective control strategy, respectively.

Fig. 10 shows the proportion of annual electricity charged to the hybrid battery systems. As shown in Fig. 10(a) and (c), vehicle batteries accounted for 85.6% and 94.1% of the total annual electricity charged in battery systems for the traditional and battery-protective control strategy, respectively. This indicates that the battery-protective control strategy was more competitive than the traditional control strategy in terms of improving the capability of shifting off-peak electricity to peak time through the vehicle battery systems. This is due to the enhancement of the battery relative capacity, which is shown in Fig. 11(a).

Fig. 11 shows the battery and the system performances in terms of different control strategies. As shown in Fig. 11 (a), by adopting the grid-responsive control strategy (i.e., the hierarchical and battery-protective control strategy), the transition of the battery degradation zone from the slow degradation zone to the acceleration zone could be prolonged from 6375 to 6750 hrs. Furthermore, compared to the hierarchical control strategy, the proposed battery-protective control strategy decreased the battery degradation rate with an improved relative capacity of batteries, i.e., the equivalent relative capacity at the end of one year's operation increased from 0.849 to 0.921, as shown in Fig. 11(a). This indicates that by removing the grid-battery charging power in the battery acceleration zone, the equivalent relative capacity could be improved. As shown in Fig. 11 (b), the implementation of the grid-battery charging in the hierarchical control resulted in an increase in the ECE from 138.3 to 144.5 kg/m^2.a (4.5%) and the annual IC from 194.3 to 210.9 HK$/m^2.a (8.5%). The underlying mechanism was that compared to the traditional control strategy, the grid-battery charging strategy increased the battery charging losses from 3.1 to 12 kWh/m^2.a. The increase in battery charging losses resulted in an increase in ECE and IC.

To characterise the relative capacity of the battery systems, parametric analysis was conducted on various renewable capacities and different values of $FSOC_{lower}$. As shown in Fig. 12(a), when the integrated wind turbine capacity was 0.2 MW, the increase in $FSOC_{lower}$ from 0.4 to 0.85 could increase the equivalent relative capacity of the battery system from 0.751 to 0.996. The underlying mechanism was that with the increase in $FSOC_{lower}$ from 0.4 to 0.85, the depth of discharge would decrease from 0.6 to 0.15, which could contribute to the decrease in the battery degradation rate, as illustrated in Fig. 8.

In addition, the comparison between the hierarchical control strategy (as shown in Fig. 12(a)) and the battery-protective control strategy (as shown in Fig. 12(b)) indicated that the equivalent relative capacity was more sensitive to the integrated wind turbine capacity in the battery-protective control strategy than in the hierarchical control strategy. For instance, when $FSOC_{lower}$ was 0.55, with the increase in the integrated wind turbine capacity from 0.2 MW to 0.8 MW, the equivalent relative capacity was increased from 0.757 to 0.758 in the hierarchical control strategy and to 0.815 in the battery-protective control strategy. Here, the underlying mechanism is that according to the grid-responsive control strategy introduced in Fig. 5, with the avoidance of a grid-battery charging strategy in the battery degradation-acceleration zone, the depth of discharge of the battery systems was more sensitive to renewable energy. Compared to the hierarchical control strategy, the battery-protective control strategy could decrease the annual average DOD from 0.527 to 0.403 when the rated capacity of the integrated wind turbine was 0.8 MW.

To comparatively investigate the system performance with respect

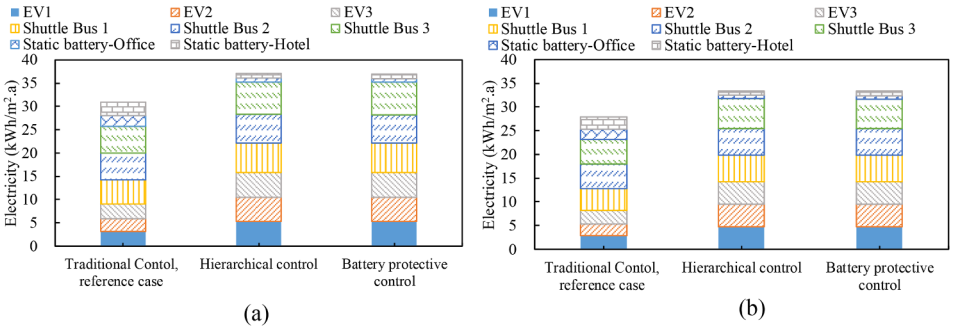

Fig. 9. Electricity flows in the static and vehicle battery systems: (a) annual total energy charged to the battery systems and (b) annual total energy discharged from the battery systems. (Note: the renewable system is BIPVs only. The lower limitation of the fractional state of charge, $FSOC_{lower}$, is 0.7, and the off-peak grid-battery charging power, $P_{G2B,off\text{-}peak}$, is 20 kW).

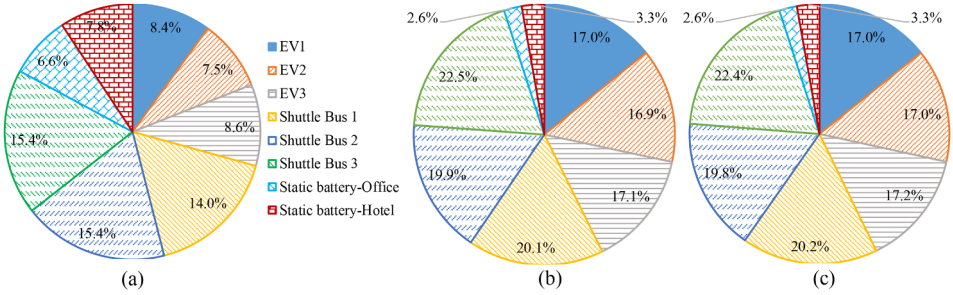

Fig. 10. Proportion of electricity in the static and vehicle battery systems: (a) traditional control strategy (reference case), (b) hierarchical control strategy, and (c) battery-protective control strategy. (Note: the renewable system is BIPVs only, the $FSOC_{lower}$ is 0.7, and the $P_{G2B,off\text{-}peak}$ is 20 kW).

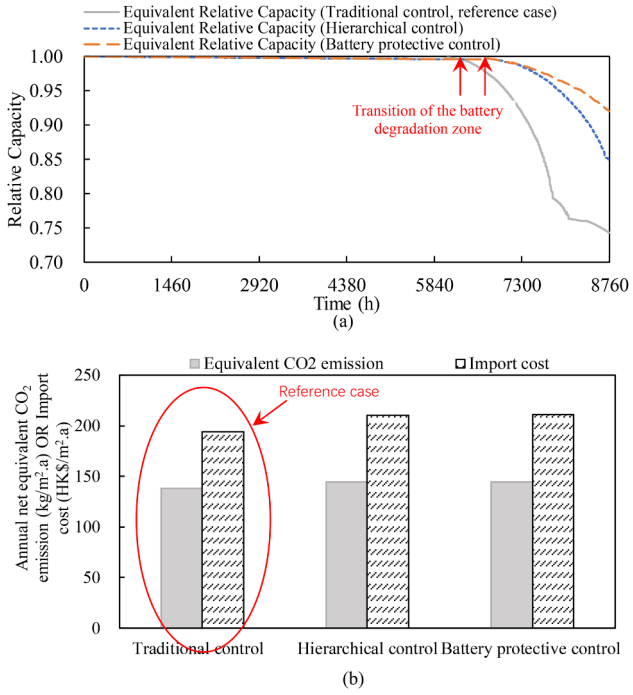

Fig. 11. Impact of different control strategies on (a) the equivalent relative capacity of the battery and the equivalent CO_2 emissions and annual import cost. (Note: the renewable system is BIPVs only, thee $FSOC_{lower}$ is 0.7, and the $P_{G2B,off\text{-}peak}$ is 20 kW).

to the proposed hierarchical and battery-protective control strategy, Fig. 13 shows the impact of $FSOC_{lower}$ on the IC and ECE. As shown in Fig. 13, when $FSOC_{lower}$ was 0.4, compared to the hierarchical control strategy with the equivalent CO_2 emissions at 94.2 kg/m^2.a, the battery-protective control strategy increased the equivalent CO_2 emissions to 94.8 kg/m^2.a. Here, the underlying mechanism was that the implementation of the battery-protective control strategy avoided the grid-battery charging in the battery degradation-acceleration zone, and the equivalent relative capacity of the batteries could be increased from 0.7511 to 0.7514. Correspondingly, the battery charging loss increased from 3.1 to 4.1 kWh/m^2.a. Furthermore, the avoidance of the grid-battery charging in the battery degradation-acceleration zone also increased the annual import cost. For instance, when $FSOC_{lower}$ was 0.4, the annual import cost was increased from 166.6 to 167.3 HK$/m^2.a. This was due to the decrease in the $E_{off\text{-}peak,grid}$ from 12.2 to 10.5 kWh/m^2.a. It can also be noted that the differences in the ECE and IC between different control strategies were smaller with respect to the increase in $FSOC_{lower}$. As shown in Fig. 13, with the increase in $FSOC_{lower}$ from 0.4 to 0.85, the difference in equivalent CO_2 emissions decreased from 0.6 to 0 kWh/m^2.a, and the difference in the IC decreased from 0.7 to 0 HK$/m^2.a. This is because the relative capacity of the battery was always within the slow degradation zone, and the relative capacity of the battery at the end of the full year was 0.996.

4.1.2. Hierarchical charging mechanism with similar charging energy in battery systems

To further investigate the effectiveness of battery-protective control strategies, the battery relative capacity was characterised and compared between different control strategies with similar charging energy in the battery systems. The motivation for this section was to quantitatively demonstrate the superiority of the battery-protective control strategy in terms of battery relative capacity and system performance under similar charging energy. To keep similar charging energies in the hybrid battery systems, both $FSOC_{lower}$ and grid-to-battery charging power were adjusted thusly: (1) in the traditional control strategy,

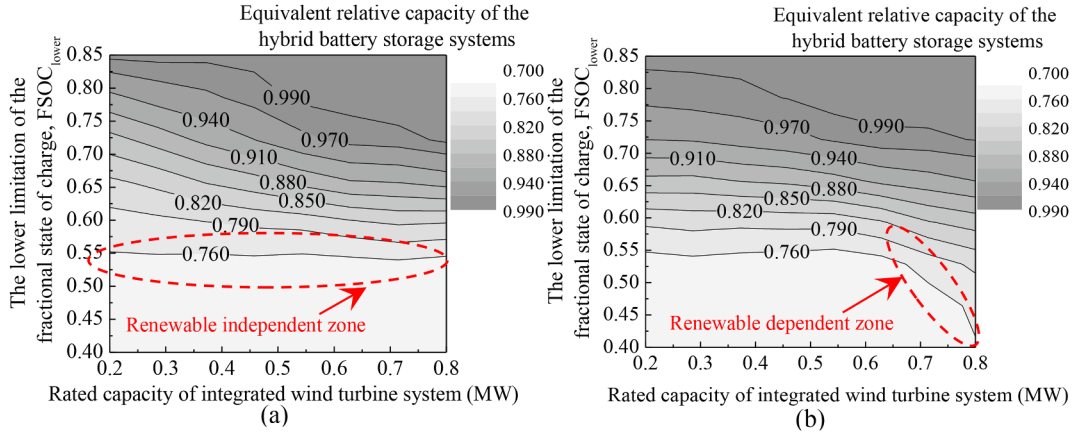

Fig. 12. Parametric analysis of rated wind turbine capacity and $FSOC_{lower}$ on the equivalent relative capacity: (a) hierarchical control strategy and (b) battery-protective control strategy.

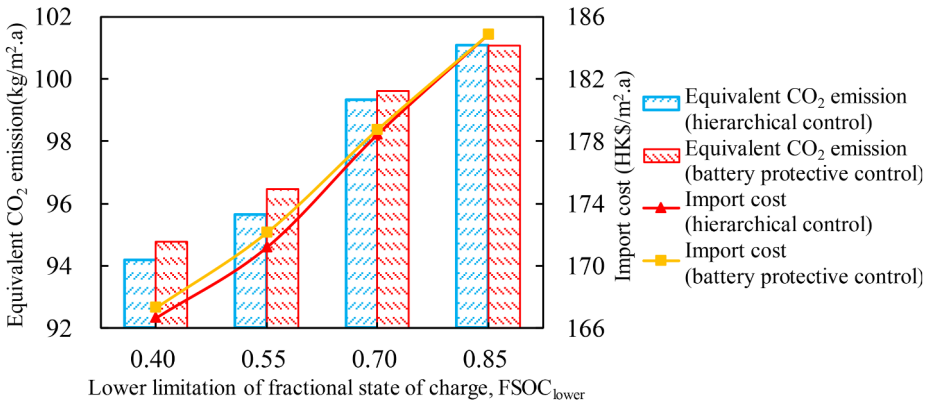

Fig. 13. Impact of $FSOC_{lower}$ on the import cost and equivalent CO_2 emissions. (Note: the integrated renewable was a hybrid solar-wind renewable system: BIPVs and a 0.2-MW wind turbine).

$FSOC_{lower}$ was kept at 0.55, (2) in the hierarchical control, $FSOC_{lower}$ and grid-to-battery charging power were approximately 0.7 and 12 kW, respectively, and (3) in the battery-protective control, $FSOC_{lower}$ and grid-to-battery charging power were approximately 0.7 and 15 kW, respectively.

Fig. 14 shows the annual electricity in hybrid batteries. As shown in Fig. 14, the total annual electricity charged to the battery systems was 31.2, 31.1, and 31.0 kWh/m^2.a for the traditional, hierarchical, and battery-protective control strategy, respectively. The total annual electricity discharged from battery systems was 28.4, 28.0, and 27.9 kWh/m^2.a for the traditional, hierarchical, and battery-protective control strategy, respectively.

Furthermore, compared to the traditional control strategy with the total annual electricity charged to static batteries (in offices and hotel) at 1.42 kWh/m^2.a, the total annual electricity charged to the static batteries in the hierarchical control and battery-protective control was much higher at 5.32 kWh/m^2.a. The underlying mechanism was that in order to shift the off-peak grid electricity to peak time, the grid-battery charging strategy was implemented to charge static batteries in the hierarchical control and battery-protective control, as introduced in Section 2.7.2 (Fig. 5). Thereafter, more off-peak grid electricity could be stored in the static batteries.

Fig. 15 shows the proportion of annual electricity charged to the hybrid battery systems. As shown in Fig. 15, compared to the traditional control strategy with the proportion of annual electricity charged to the static batteries (in offices and hotel) at 4.5%, the proportions of annual electricity charged to the static batteries in the grid-responsive control strategy, as shown in Fig. 15(b) and (c), were much higher at 17.1% and 17.2%, respectively. Meanwhile, the vehicle batteries accounted for more than 80% of the total annual electricity charged in battery systems. This indicates that the integration of vehicle battery systems in building energy systems is promising in terms of shifting off-peak electricity to peak time.

As shown in Fig. 16(a), by adopting the grid-responsive control strategy (i.e., the hierarchical and battery-protective control strategy), the transition of the battery degradation zone from the slow degradation zone to the acceleration zone could be prolonged from 7625 to 8125 hrs. Furthermore, compared to the hierarchical control strategy, the proposed battery-protective control strategy decreased the battery degradation rate with an improved equivalent relative capacity. For instance, compared to the equivalent relative capacity at 0.94 and 0.98 in the traditional control strategy and hierarchical control strategy, respectively, the equivalent relative capacity could be increased to 0.986 in the battery-protective control strategy. This indicates that by removing the grid-battery charging power in the acceleration zone, the equivalent relative capacity could be improved. The underlying mechanism was that compared to the traditional control strategy, the proposed battery-protective control strategy reduced the energy charged to the vehicle systems from 30.2 to 25.7 kWh/m^2.a.

It can also be noted that compared to the case with the same settings of charging power and $FSOC_{lower}$, as shown in Fig. 11, the effectiveness of the battery-protective control strategy on the improvement of equivalent relative capacity was less obvious in the case with nearly the same charging energy. To be more specific, compared to the increasing magnitude of equivalent relative capacity from 0.743 to 0.921, as shown in Section 4.1.1 (Fig. 11), the increasing magnitude of equivalent relative capacity was less obvious, from 0.940 to 0.986. This is due to the difference in total energy charged to the battery systems between different control strategies, i.e., 6 kWh/m^2.a (from 37 to 31 kWh/m^2.a) in the case with the same settings of charging power and $FSOC_{lower}$, as shown in Fig. 11, and 0.6 kWh/m^2.a (from 28.5 to 27.9 kWh/m^2.a) in the case with nearly the same charging energy.

Fig. 16 (b) indicates that the implementation of the battery-protective control strategy decreased the ECE from 144.5 to 143.1 kg/m^2.a and the IC from 211 to 201.4 HK$/$m^2$.a. The reason for the similar equivalent CO_2 emissions between different control strategies was due to the virtually similar battery charging losses of approximately 2.8 kWh/m^2.a. The reason for the IC saving was due to the

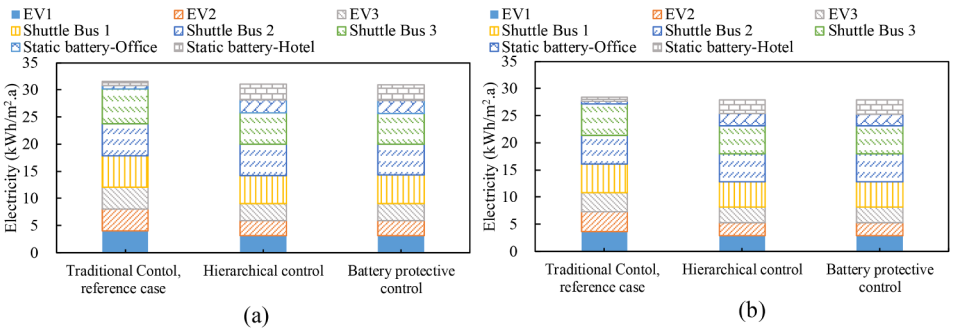

Fig. 14. Electricity flows in the static and vehicle battery systems: (a) annual total energy charged to the battery systems and (b) annual total energy discharged from the battery systems. (Note: the renewable system was BIPVs only. In the traditional control strategy, $FSOC_{lower}$ was kept at 0.55. $FSOC_{lower}$ and grid-to-battery charging powers were approximately 0.7 and 12 kW, respectively, for the hierarchical control. $FSOC_{lower}$ and grid-to-battery charging powers were approximately 0.7 and 15 kW, respectively, for the battery-protective control.)

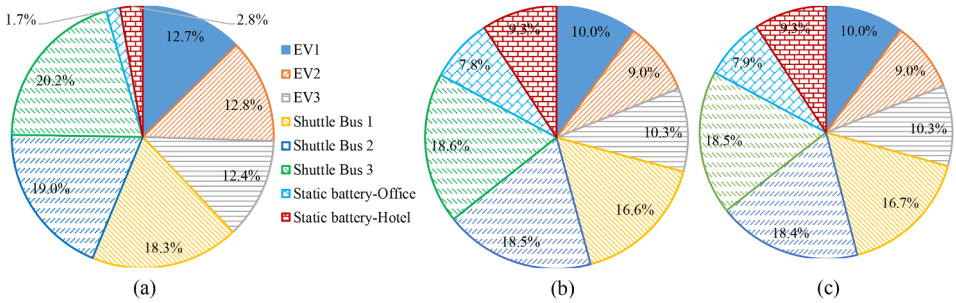

Fig. 15. Proportion of electricity in the static and vehicle battery systems: (a) traditional control strategy (reference case), (b) hierarchical control strategy, and (c) battery-protective control strategy.

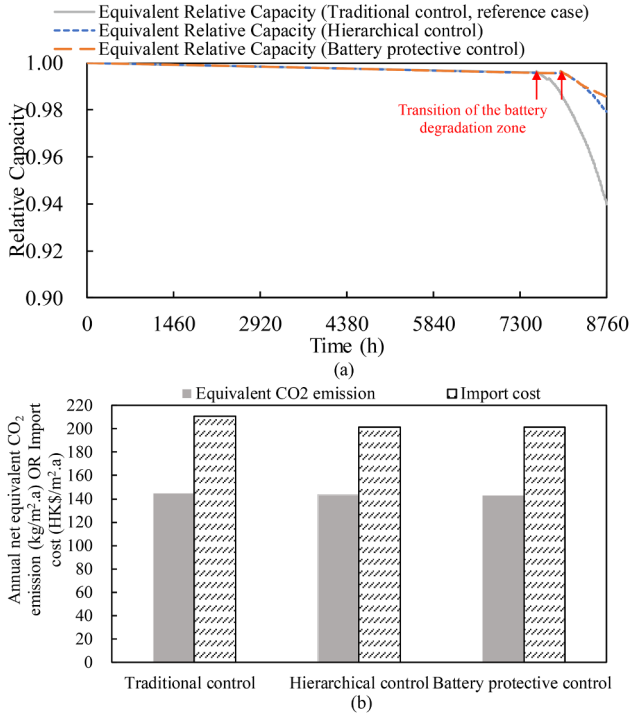

Fig. 16. Effect of control strategies on (a) equivalent relative capacity of the battery and (b) ECE and annual import cost. (Note: the renewable system was BIPVs only. In the traditional control strategy, $FSOC_{lower}$ is kept at 0.55. $FSOC_{lower}$ and grid-to-battery charging power were approximately 0.7 and 12 kW, respectively, for the hierarchical control. FSOClower and grid-to-battery charging power were approximately 0.7 and 15 kW, respectively, for the battery-protective control.)

improvement of the relative capacity from 0.940 to 0.986, as shown in Fig. 16 (a).

4.2. Sensitivity analysis of the battery-protective control strategy

Based on the above discussions, a critical contradiction can be noticed: the grid-battery charging process improved the depth of discharge and thus slowed the battery depreciation rate, whereas the grid-battery charging process led to an increase in the number of cycles together with battery degradation. In this section, parametric analysis was conducted specifically for the battery-protective control strategy, to provide technical guidance to system operators in terms of this contradiction.

4.2.1. Impact of the off-peak grid-battery charging power and the lower limitation of the fractional state of charge on system performance and battery depreciation

Parametric analysis results of the equivalent CO_2 emissions, economic performance, flexibility, and battery relative capacity are shown in Fig. 17 in terms of the off-peak grid-battery charging power ($P_{G2B,off\text{-}peak}$) and $FSOC_{lower}$. As shown in Fig. 17 (a) and Fig. 17 (b), when $P_{G2B,off\text{-}peak}$ was 5 kW, the increase in $FSOC_{lower}$ from 0.4 to 0.85 increased the ECE from 139.6 to 146.1 kg/m^2.a and the IC from 200.1 to 214 HK$/m^2.a. The underlying mechanism was due to the increase in battery charging loss from 3.7 to 12.2 kWh/m^2.a. Furthermore, both the ECE and IC were less sensitive to $P_{G2B,off\text{-}peak}$ in terms of increasing $FSOC_{lower}$. This was indicated by the flattened contour curve shown in Fig. 17 (a) and (b). This is because with the increase in $FSOC_{lower}$, the grid-battery charging process in the slow degradation zone could reduce the depth of discharge and thus slow the battery depreciation rate. The similar value of equivalent battery relative capacity with respect to $P_{G2B,off\text{-}peak}$, as shown in Fig. 17 (e), made the total energy charged to the battery system less sensitive to $P_{G2B,off\text{-}peak}$ (at approximately 37 kWh/m^2.a). Regarding the contradiction resulting from the grid-battery charging, such as the deceleration of the battery depreciation rate (due to the decrease in DOD) and the real-time battery degradation (due to the increase in the number of cycles), a trade-off could be reached when $FSOC_{lower}$ was 0.7.

As for the energy flexibility in the formulated interactive energy sharing network, as shown in Fig. 17 (c) and (d), when $P_{G2B,off\text{-}peak}$ was 10 kW, with the increase in $FSOC_{lower}$ from 0.4 to 0.85, the off-peak RSR was reduced from 0.332 to 0.177 and the off-peak GSR was reduced from 0.0719 to 0.0667. The underlying reason for the decrease in the RSR was that as the battery storage capacity was limited, the increase in $FSOC_{lower}$ from 0.4 to 0.85 reduced $E_{off\text{-}peak,REe}$ from 12.6 to 6.8 kWh/m^2.a. The underlying reason for the decrease in the GSR was that the increase in $FSOC_{lower}$ from 0.4 to 0.85 reduced $E_{off\text{-}peak,grid}$ from 18.2 to 16.8 kWh/m^2.a. Furthermore, when $FSOC_{lower}$ was 0.4, the increase in $P_{G2B,off\text{-}peak}$ from 5 to 20 kW resulted in a decrease in RSR from 0.410 to 0.222 and an increase in GSR from 0.0573 to 0.0847. The underlying reason for the decrease in RSR was that as the battery storage capacity was limited, the increase in $P_{G2B,off\text{-}peak}$ from 5 to 20 kW reduced $E_{off\text{-}peak,REe}$ from 16.6 to 8.9 kWh/m^2.a. The underlying reason for the increase in GSR was that the increase in $P_{G2B,off\text{-}peak}$ from 5 to 20 kW increased $E_{off\text{-}peak,grid}$ from 18.2 to 21.3 kWh/m^2.a.

With respect to the equivalent relative capacity, as shown in Fig. 17 (e), the equivalent relative capacity was highly dependent on $FSOC_{lower}$ and was less sensitive to $P_{G2B,off\text{-}peak}$. This indicated that when operating the battery storage system, $FSOC_{lower}$ should be given priority for consideration to reduce battery degradation during charging/discharging cycles.

As shown in Fig. 17 (f), it is noteworthy that in terms of energy management through $P_{G2B,off\text{-}peak}$ and $FSOC_{lower}$, the increase in equivalent relative capacity increased GSR but decreased RSR. In the $P_{G2B,off\text{-}peak}$-dependent scenarios, with an increase in equivalent relative capacity from 0.8505 to 0.8569, GSR increased from 0.0573 to 0.0847, whereas RSR decreased from 0.41 to 0.222. This because with the increase in $P_{G2B,off\text{-}peak}$ from 5 to 20 kW, $E_{off\text{-}peak,grid}$ increased from 18.2 to 25.3 kWh/m^2.a, whereas $E_{off\text{-}peak,REe}$ decreased from 12.6 to

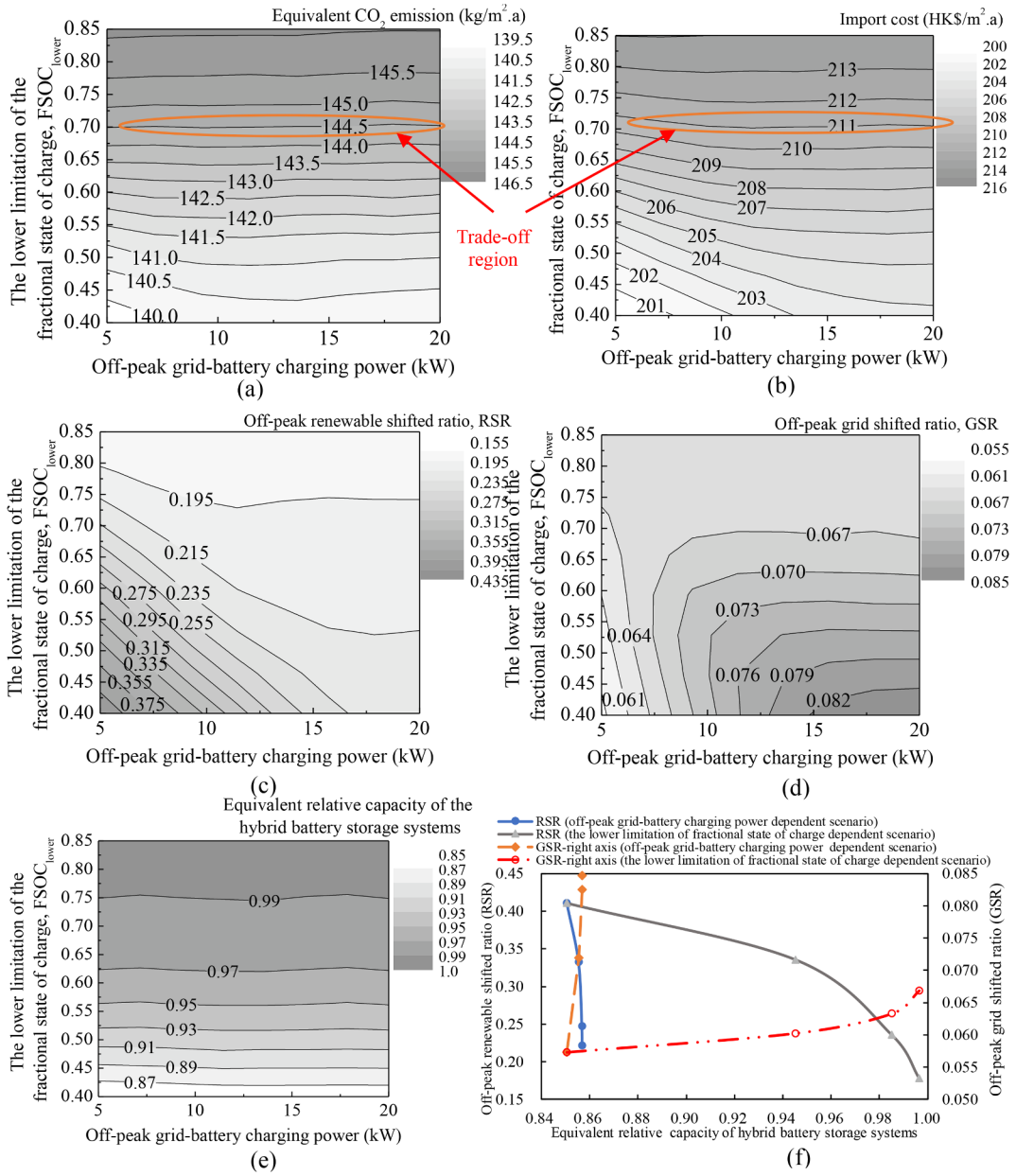

Fig. 17. Effect of off-peak grid-battery charging power ($P_{G2B,off\text{-}peak}$) and $FSOC_{lower}$ on: (a) equivalent CO_2 emissions, (b) annual import cost, (c) off-peak RSR, (d) off-peak GSR, (e) equivalent relative capacity of the battery, and (f) impact of battery depreciation on energy flexibility. (Note: the renewables–buildings–vehicles system was only supported by BIPVs).

10.8 kWh/m^2.a. In the $FSOC_{lower}$-dependent scenarios, with the increase in equivalent relative capacity from 0.8505 to 0.9964, GSR increased from 0.0573 to 0.0668, whereas RSR decreased from 0.41 to 0.178. This was because with the increase in $P_{G2B,off\text{-}peak}$ from 5 to 20 kW, $E_{off\text{-}peak,grid}$ increased from 18.2 to 29.6 kWh/m^2.a, whereas $E_{off\text{-}peak,REe}$ decreased from 12.6 to 9.2 kWh/m^2.a.

4.2.2. Impact of static battery and integrated wind turbine on system performance and battery depreciation

Parametric analysis results of ECE, economic performance, energy flexibility, and equivalent relative capacity of batteries are shown in Fig. 18. Note that the increase in the static battery capacity increased the ECE and decreased the annual IC. For instance, as shown in Fig. 18(a) and (b), when the renewable capacity was 0.2 MW, with the increase in static battery capacity of each floor from 3 to 15 kWh, the ECE increased from 98.3 to 100 kg/m^2.a, whereas the IC decreased from 180.3 to 170.1 HK$/m^2.a. The underlying reason for the increase in equivalent CO_2 emissions was due to the increase in battery charging loss from 3.4 to 5.8 kWh/m^2.a, whereas the decrease in the annual import cost was due to the increase in RSR from 0.131 to 0.132, as shown in Fig. 18 (c), and the increase in GSR from 0.03 to 0.05, as shown in Fig. 18 (d).

Regarding the equivalent relative capacity, as shown in Fig. 18 (e), the increase in battery storage capacity and integrated wind turbine capacity increased the equivalent relative capacity. This is because, with respect to the increase in renewable capacity, the discharging cycles of the battery storage system were reduced, as the demand could be directly covered by the integrated renewable generation. Furthermore, the increase in the static battery capacity reduced the number of cycles, thus prolonging the relative capacity of the battery. These results can guide system managers to decelerate battery degradation and provide economic viability to the interactive renewables–buildings–vehicles energy-sharing network.

As shown in Fig. 18 (f), in terms of energy management through the

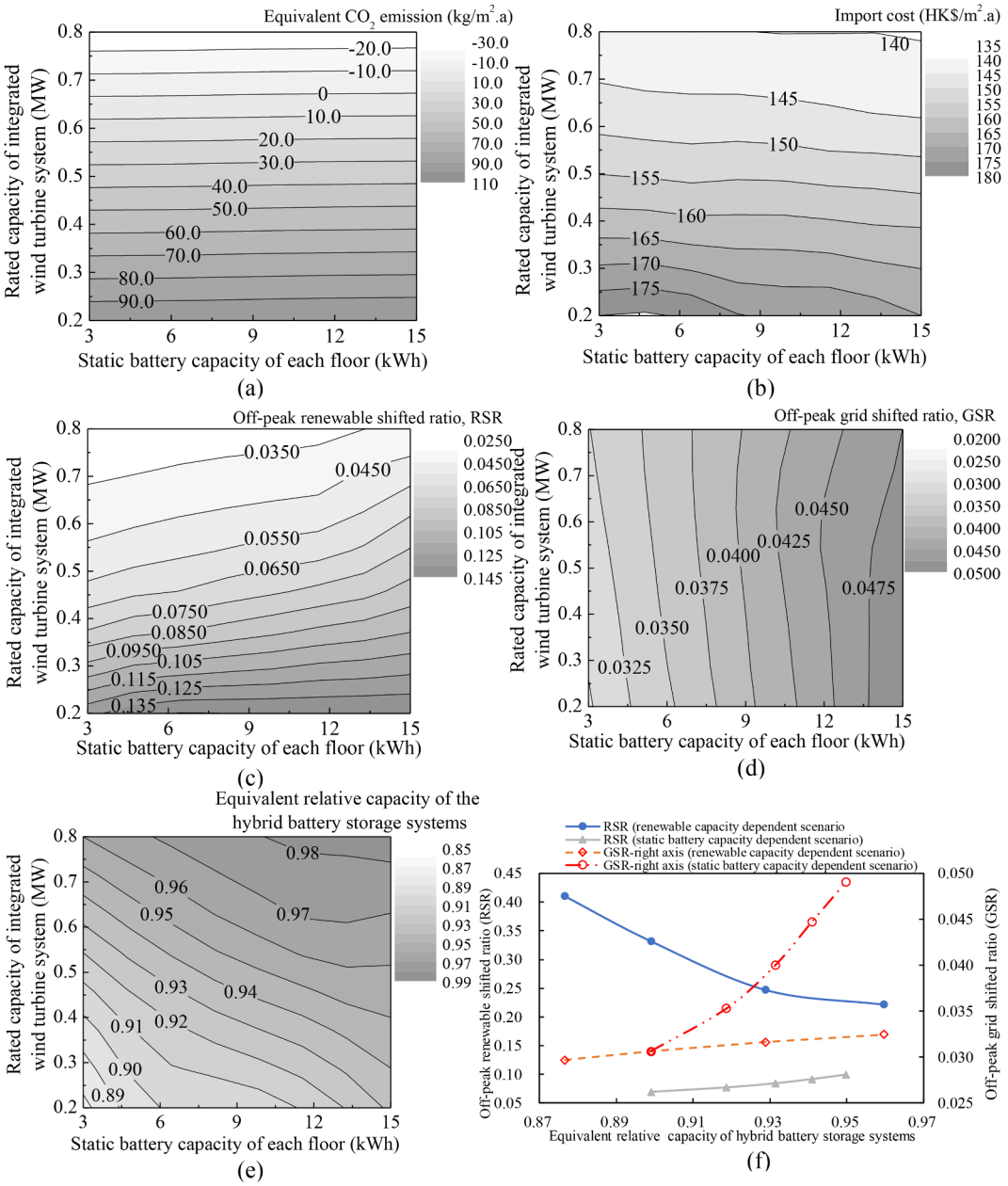

Fig. 18. Impact of the static battery capacity and integrated renewable capacity on (a) equivalent CO_2 emission, (b) annual import cost, (c) off-peak RSR, (d) off-peak GSR, (e) the equivalent relative capacity of the batteries, and (f) the impact of battery depreciation on energy flexibility. (Note: the renewables–buildings–vehicles system was only supported by BIPVs for (f). The charging power was 20 kW and $FSOC_{lower}$ was 0.7).

integrated wind turbine capacity and static battery capacity, the impact of battery depreciation on energy flexibility indexes was complicated. In the static battery capacity-dependent scenarios, with the increase in equivalent relative capacity from 0.899 to 0. 95, GSR increased from 0.0306 to 0.0491 and RSR increased from 0.0689 to 0.0992. This is because with the increase in the static battery capacity from 3 to 15 kWh, $E_{off\text{-}peak,grid}$ increased from 10.3 to 14.8 kWh/m^2.a and $E_{off\text{-}peak,REe}$ decreased from 10.9 to 17.6 kWh/m^2.a. In the renewable capacity-dependent scenarios, with the increase in equivalent relative capacity from 0.877 to 0.96, GSR increased from 0.0297 to 0.0324, whereas RSR decreased from 0.410 to 0.222. The reason for this is that with the increase in integrated wind turbine capacity from 0.2 to 0.8 MW, $E_{surp,REe}$ increased from 3.6 to 90.8 kWh/m^2.a, whereas $E_{off\text{-}peak,grid}$ increased from 15.7 to 28.2 kWh/m^2.a.

Fig. 19 demonstrates the parametric analysis of the static battery capacity and integrated renewable capacity. With respect to the increase in the static battery capacity from 3 to 15 kWh, the equivalent CO_2 emission was improved from 14 to 15.5 kg/m^2.a (as shown in Fig. 19(a)), whereas the annual import cost decreased from 148.6 to 147 HK$/$m^2$.a (as shown in Fig. 19(c)). The underlying mechanism is due to the increased battery charging loss from 9.6 to 11.7 kWh/m^2.a. From the perspective of energy flexibility, as shown in Fig. 19(f), the increase in the static battery capacity from 3 to 15 kWh will result in an increase in the RSR from 0.042 to 0.067 and increase in the GSR from 0.032 to 0.048. This indicates that the increase in the static battery capacity will contribute to the improvement of renewable electricity and grid electricity stored during the off-peak periods. However, the increase in the renewable capacity (from 0.2 to 0.8 MW) will reduce the ECE (from 100.5 to –23 kg/m^2.a, as shown in Fig. 19(b)) and the import cost (from 172.7 to 139.3 HK$/$m^2$.a, as shown in Fig. 19(b)), whereas the energy flexibility is decreased (RSR is decreased from 0.131 to 0.056, as shown in Fig. 19(d), and GSR is decreased from 0.050 to

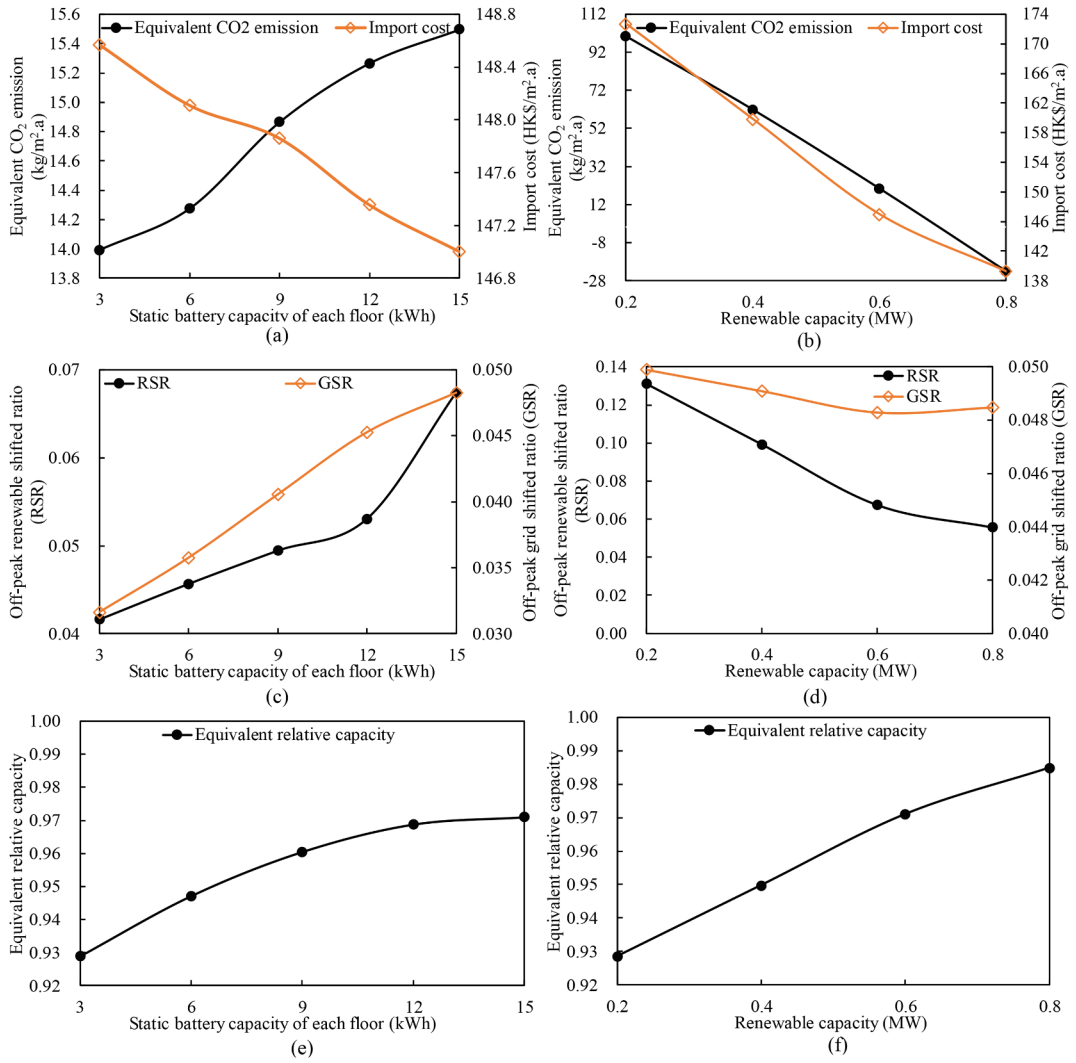

Fig. 19. Multi-criteria performances of the interactive buildings–vehicles system with respect to the (a)(c)(e) static battery capacity and (b)(d)(f) integrated renewable capacity.

0.049, as shown in Fig. 19(d)). The reason is similar to that of Fig. 18. It is noteworthy that effective solutions for the relative capacity improvement include the enhancement of the static battery capacity and integrated renewable capacity.

4.2.3. Uncertainty and sensitivity analysis on mobile battery capacity

Fig. 20 demonstrates the impact of mobile battery capacity on the multi-criteria performances of the interactive buildings–vehicles system. As shown in Fig. 20, the increase in the mobile battery capacity will result in a decrease in the import cost, increase in the ECE, and increase in the energy flexibility indicators. Furthermore, an almost saturated tendency can be noticed when the mobile battery capacity of electric vehicle is increased to 60 kWh (as shown in Fig. 20(a)(c)) and the shuttle bus to 70 kWh (as shown in Fig. 20(b)(d)). This is mainly due to the almost saturated total energy charged in the battery systems at 35.3 kWh/m^2.a, which is independent of the further increase in the mobile battery capacity. It is noteworthy that the enhancement of the mobile battery capacity can also be an effective solution for the improvement of equivalent relative capacity (as shown in Fig. 20(e, f)).

4.2.4. Uncertainty and sensitivity analysis on equivalent CO_2 emission factor (CEF_{eg}) and electricity price

Fig. 21 shows the impact of different equivalent CO_2 emission factors (CEF_{eg}) and grid electricity prices on multi-criteria performances of the interactive buildings–vehicles system. As shown in Fig. 21(a), for a nearly zero-energy buildings–vehicles system, the decrease in CEF_{eg} from 0.9 to 0.1 kg/kWh will contribute to the decrease in the ECE from 19.9 to 2.2 kg/m^2.a by 88.9%. This indicates that the transition from the carbon coal powered dirty grid to the renewable powered cleaner grid is fairly necessary for the promotion of the renewable and sustainable buildings–vehicles system. Meanwhile, the import cost is independent on CEF_{eg} at 147 HK$/$m^2$.a. Furthermore, as shown in Fig. 21(b), the decrease in grid electricity price from 1.5 to 0.3 HK $/kWh will contribute to a decrease in import cost from 245 to 49 HK $/$m^2$.a by 80%. This indicates that solutions for the decrease in the grid electricity price are fairly necessary for the promotion of the economically competitive buildings–vehicles system. It is also noteworthy that the ECE is independent of the grid electricity price at 15.5 kg/m^2.a.

5. Research results comparison and accuracy assessment

In comparison with the research results in academia, the import cost is more sensitive to the grid electricity price. For instance, with an increase in grid electricity price from 0.3 to 0.9 HK$/kWh, the import cost will be increased from 78.5 to 112 HK$/$m^2$.a [37], whereas a more obvious increase can be noticed from 49 to 245 HK$/$m^2$.a in this study. The main reason for this is that the aggregated demands of buildings in this study are much higher than the demand of a single office building

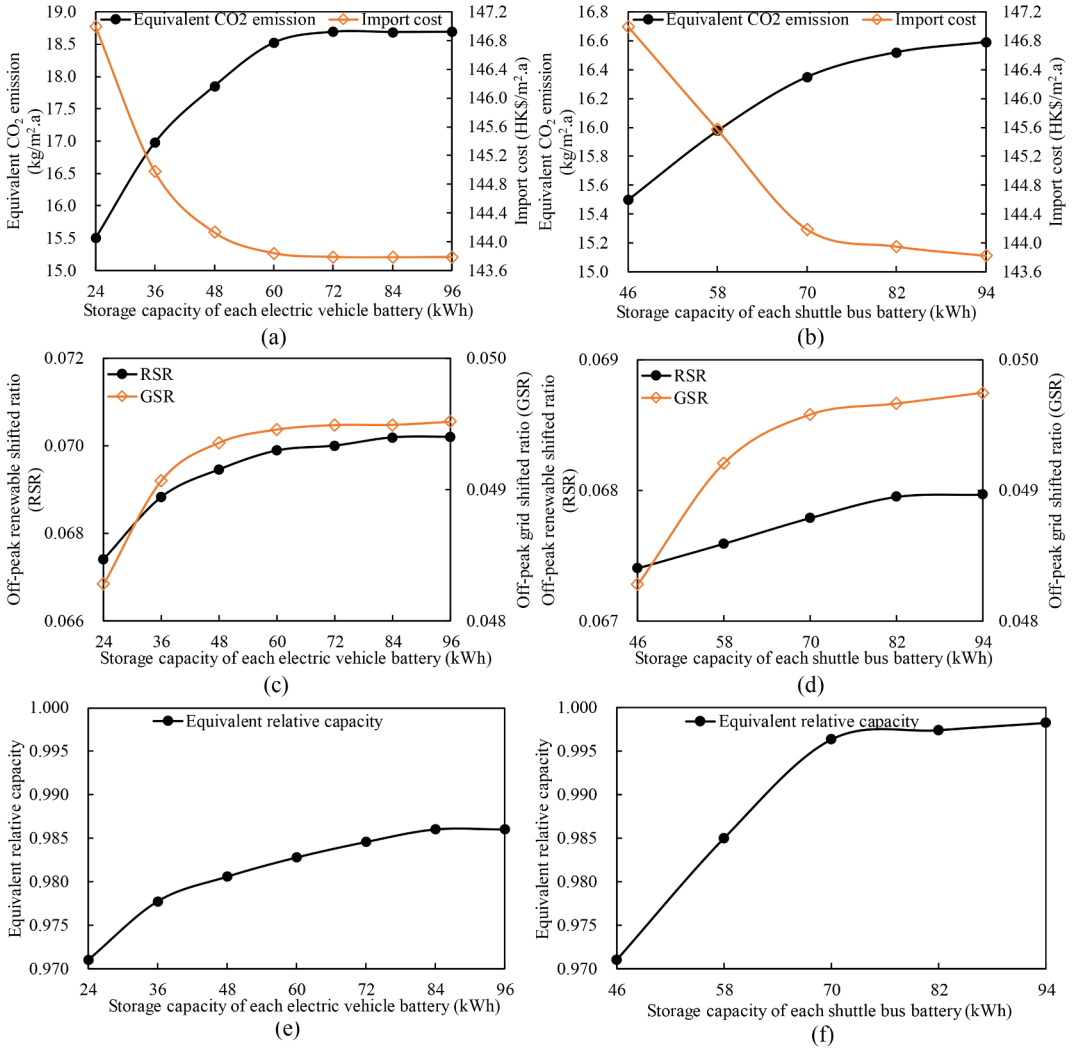

Fig. 20. Uncertainty and sensitivity analysis on multi-criteria performances of the interactive buildings– vehicles system with respect to mobile battery capacity of (a) (c)(e) EVs and (b)(d)(f) shuttle buses. (Note: the integrated renewable capacity is a 0.6-MW wind turbine system).

in [37]. Furthermore, with the increase in the renewable capacity from 0.2 to 0.8 MW, the ECE will be decreased from approximately 30 to −110 kg/m^2.a in [37], whereas a more slight decrease can be noticed from 100 to –23 HK$/m^2.a in this study. This is mainly due to the higher battery charging losses of the aggregated buildings–vehicles system in this study than the single building–vehicles system in [37]. Furthermore, according to research results [55-60], the increase in the renewable penetration will reduce the operation cost and ECE, whereas the increase in the battery charging losses will result in the increase in ECE.

From the perspective of energy flexibility, in order to improve the Zhou and Cao [61] adopted integrated solutions to enhance the building energy flexibility, including hybrid thermal and electric storages and diversified energy conversion strategies. Results indicated that, through the integrated thermal and electrical storage systems, the enhancement of the storage capacity will improve the on-site flexible

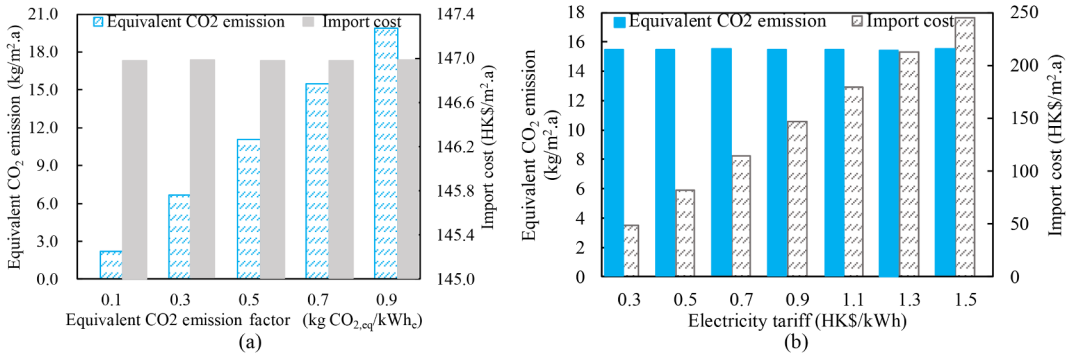

Fig. 21. Uncertainty and sensitivity analysis on multi-criteria performances of the interactive buildings– vehicles system with respect to (a) different equivalent CO_2 emission factors and (b) grid electricity prices. (Note: the integrated renewable capacity is a 0.6-MW wind turbine system.)

surplus renewable fraction ratio and the on-site flexible electric load fraction. The conclusions of this study find a similar trend but with different magnitudes, as in academia [37], i.e., the increase in battery capacity will increase the GSR, whereas the increase in the integrated renewable capacity will reduce the RSR and GSR. The reason for the different magnitudes is mainly due to the expansion of the system energy boundary and the implemented battery-protective control strategy. Furthermore, the increase in the grid-battery charging power will increase the GSR but decrease the RSR. In addition, the increase in the battery storage will reduce the grid's reliance, similar to the results in [62].

The academic literature also indicates that, the multi-criteria performances (the energy matching between renewable and demand, the operational cost and so on) are highly dependent on the battery degradation and the battery energy management strategy. Salpakari et al. [32] indicated that, the neglection of battery degradation will overestimate the V2B cost saving, although the renewable penetration can be increased. Aelenei et al. [63] studied the energy flexibility provided by the battery energy storage systems coupled with vertical BIPV and rooftop PV systems. Research results indicated that, a 13.5 kWh battery can realise the positive net present value of 1416.1 EUR, with the self-consumption and self-sufficiency ratios at 56.3% and 62.4%, respectively. Phan et al. [64] optimised the battery charging and discharging rate to reduce the operational cost. With the adoption of the genetic algorithm, the average daily operating cost can be reduced by 31%. Liu et al. [65] conducted the multi-objective optimisation on charging modes (charging speed, energy conversion efficiency as well as temperature variations) for intelligent battery management, in respect to the charging time, energy loss and temperature rise. The proposed Pareto fronts-based solutions can provide technical guidance to system operators.

From the perspective of the adopted technology, the latest research works also indicate that the effective strategies for techno-economic performance improvement of integrated building energy systems include integrated PV-thermal systems [59], energy sharing technology in buildings and districts [60], V2B interactions [18,25], and grid-responsive control strategies [66]. Khatib et al. [67] conducted the comprehensive and systematic literature review on optimal sizing methods for PV and battery systems. The adopted methods include the software tools, numerical methods and artificial intelligence methods. Compared to the other methods, the artificial intelligence methods are more efficient due to the large search space and high computational efficiency. These latest technologies support the research results in this study.

6. Research applications, limitations, and future studies

This study thoroughly investigated the techno-economic performances of a grid-connected buildings–vehicles system with multi-directional energy interactions, comprehensively considering the cycling aging of battery storage during frequent charging/discharging cycles. A mathematical model was developed to characterise the cycling aging of electrochemical battery storage. An advanced battery-protective energy control strategy was developed that fully utilises inherent battery depreciation characteristics for flexible energy management. In terms of the advanced battery-protective energy control strategy, the grid-battery charging process can decrease the depth of discharge and thus slow down the battery depreciation rate, whereas the grid-to-battery charging will accelerate the cycling aging. The proposed techniques can be widely applied in the energy management of district ZEB and ZEV systems, grid-responsive power control, battery-protective solutions, and more. However, the calendar aging of battery systems has not been considered in this study. Furthermore, the development of the dynamic off-peak grid-to-battery charging strategy, in accordance with the dynamic renewable-demand signal and dynamic relative capacity signal of battery systems, has not been developed, especially considering the increase in acceleration rate of battery cycling aging with the increase in the number of cycles. Future studies will be focused on mathematical model development of battery degradation, including calendar aging and cycling aging. Furthermore, the development of a metaheuristic self-learnt grid-to-battery charging strategy will be investigated by dynamically adjusting the off-peak grid-to-battery charging power in accordance with the dynamic renewable-demand signal and dynamic relative capacity signal of battery systems.

7. Conclusions

In this study, a resilient energy network called the interactive renewables–buildings–vehicles energy sharing network was managed through a centralised collaborative controller for renewable energy and grid electricity in response to the coverage of both mobility consumption and energy demands of buildings. A mathematical model was developed to characterise the real-time battery degradations for multi-directional energy interactions, including buildings-to-vehicles, vehicles-to-buildings, grid-to-buildings, buildings-to-grid, and grid-to-vehicles. A comparison between a bivariate mathematical fitting method and a single-variable mathematical fitting method with piecewise fitting was conducted to accurately characterise the cycling aging of battery storage in terms of the number of cycles and depth of discharge. To reduce the battery depreciation rate in the multidirectional energy interaction process, a heuristic battery-protective energy control strategy was developed by allocating resilient and flexible grid-to-battery charging schemes according to the inherent battery depreciation characteristics (i.e., renewable-battery charging, grid-battery charging in the slow degradation zone, and the avoidance of grid-battery charging in the acceleration zone). The developed battery-protective energy control strategy was thereafter compared with traditional and hierarchical control strategy to show its reliability and robustness in terms of multi-criteria performance enhancements (including equivalent CO_2 emission, import cost, system energy flexibility, and relative battery capacity). With respect to battery depreciation, a critical energy contradiction was presented, i.e., that the grid-battery charging process improved the depth of discharge and thus slowed the battery depreciation rate, whereas the grid-battery charging process led to an increased number of cycles together with battery degradation. This was discussed together with effective technical solutions. To provide technical guidance to system designers, operators, and stakeholders, a systematic and comprehensive analysis was conducted on associated parameters, including off-peak grid-battery charging power, the lower limitation of the fractional state of charge, battery capacity, and renewable capacity. The main conclusions are as follows:

1) With respect to the accuracy of the developed mathematical model, compared to the bivariate mathematical fitting method with the highest R^2 of 0.9206, the single-variable mathematical fitting method with piecewise fitting curves shows more robustness and reliability with R^2 of 0.9807.
2) In the grid-connected buildings–vehicles system, the proposed grid-responsive strategy can improve the equivalent relative capacity of battery systems through the mechanism for the decrease in the depth of discharge. Depending on the resilient and flexible grid-to-battery charging scheme, the grid-responsive strategy includes the hierarchical control strategy and battery-protective control strategy. In the scenario with the same settings of charging power and lower limitation of fractional state of charge, compared to traditional control strategies, the equivalent relative capacity can be increased from 0.743 to 0.849 when adopting the hierarchical control strategy and be further increased to 0.921 when adopting the battery-protective control strategy. In the scenario with the same settings of charging energy in battery systems, compared to traditional control strategies, the equivalent relative capacity can be increased from 0.94 to 0.98 in the hierarchical control strategy and be further

increased to 0.986 when adopting the battery-protective control strategy.

3) With respect to the battery-protective control strategy, a contradiction can be observed, i.e., the grid-battery charging process can improve the depth of discharge and thus slow the battery depreciation rate, whereas the grid-battery charging process will lead to an increase in the number of cycles together with battery degradation. A trade-off can be reached with $FSOC_{lower}$ at 0.7, where the relative capacity is not sensitive to the off-peak grid-battery charging power. Furthermore, due to the decrease in the number of cycles, the increase in battery storage capacity can also increase the equivalent relative capacity. Other technical solutions for the improvement in battery relative capacity include increasing the lower limitation of the fractional state of charge and increasing renewable capacity.
4) In terms of intelligent battery energy management through the off-peak grid-battery charging power and $FSOC_{lower}$, the increase in the equivalent relative capacity will increase the off-peak GSR but decrease the off-peak surplus RSR. In the off-peak grid-battery charging power-dependent scenarios, with the increase in the equivalent relative capacity from 0.8505 to 0.8569, GSR increases from 0.0573 to 0.0847, whereas RSR decreases from 0.410 to 0.222. In $FSOC_{lower}$-dependent scenarios, with the increase in equivalent relative capacity from 0.8505 to 0.9964, GSR increases from 0.0573 to 0.0668, while RSR decreases from 0.410 to 0.178.
5) With respect to energy flexibility, in terms of energy management through the integrated wind turbine capacity and static battery capacity, the impact of battery depreciation on energy flexibility indexes is complicated. In the static battery capacity-dependent scenarios, with the increase in equivalent relative capacity from 0.899 to 0.950, GSR increases from 0.0306 to 0.0491, and RSR increases from 0.0689 to 0.0992. In the renewable capacity-dependent scenarios, with the increase in equivalent relative capacity from 0.877 to 0.96, GSR increases from 0.0297 to 0.0324, while RSR decreases from 0.410 to 0.222.

Future studies will be focused on mathematical model development of battery degradation, including calendar aging and cycling aging. Furthermore, the development of a metaheuristic self-learnt grid-to-battery charging strategy will be investigated by dynamically adjusting the off-peak grid-to-battery charging power in accordance with the dynamic renewable-demand signal and dynamic relative capacity signal of battery systems.

CRediT authorship contribution statement

Yuekuan Zhou: Conceptualization, Methodology, Investigation, Writing - original draft, Writing - review & editing. **Sunliang Cao:** Supervision, Funding acquisition, Project administration, Conceptualization, Methodology, Investigation, Writing - original draft, Writing - review & editing. **Jan L.M. Hensen:** Investigation, Writing - original draft, Writing - review & editing. **Ala Hasan:** Investigation, Writing - original draft, Writing - review & editing.

Declaration of Competing Interest

The authors declare that they have no known competing financial interests or personal relationships that could have appeared to influence the work reported in this paper.

Acknowledgement

This research is supported by the HK RGC (Hong Kong Research Grants Council) Research Project 25215618 (The optimal transitions from interactively-isolated systems to mutually-integrated unity between zero-energy building(s) and zero-energy vehicle(s)).

Appendix A

.

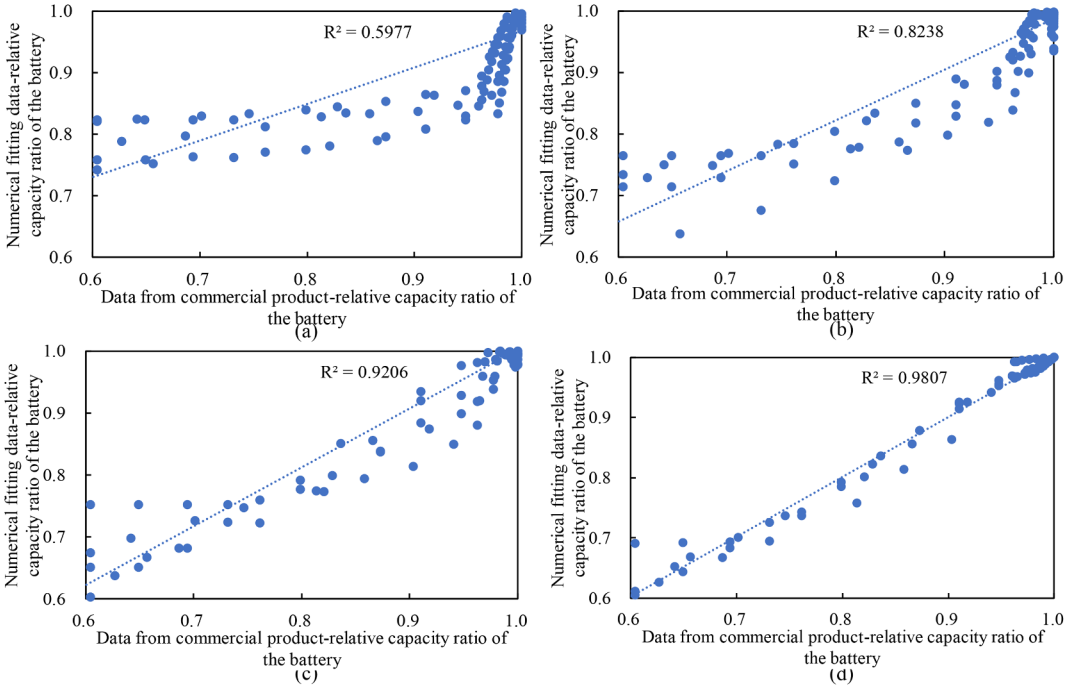

Fig. 22. (a–c) Correlation analysis of relative capacity using the bivariate mathematical fitting method and (d) correlation analysis of relative capacity using the single-variable mathematical fitting method with piecewise fitting curves.

References:

[1] HKEED (Hong Kong Energy End-use Data). 2018. “Hong Kong Energy End-use Data 2018.” https://www.emsd.gov.hk/filemanager/en/content_762/HKEEUD2018.pdf.
[2] Jensen SØ, Marszal-Pomianowska A, Lollini R, Pasuy W, Knotzer A, Engelmann P, et al. IEA EBC Annex 67 Energy Flexible Buildings. Energy Build 2017;155:25–34.
[3] Stavrakas V, Flamos A. A modular high-resolution demand-side management model to quantify benefits of demand-flexibility in the residential sector. Energy Convers Manage 2019. https://doi.org/10.1016/j.enconman.2019.112339.
[4] Finck C, Li R, Kramer R, Zeiler W. Quantifying demand flexibility of power-to-heat and thermal energy storage in the control of building heating systems. Appl Energy 2017;209:409–25.
[5] Junker R, Azar A, Lopes RA, Lindberg K, Reynders G, Relan R, et al. Characterizing the energy flexibility of buildings and districts. Appl Energy 2018;225:175–82.
[6] Selinger-Lutz O, Pratidino G, Hollinger R, Fischer D, Koch B, Wittwer C. Flexibility assessment of a pool of residential micro combined heat and power systems. Energy Convers Manag 2018;172:228–36.
[7] Reynders G, Diriken J, Saelens D. Generic characterization method for energy flexibility: Applied to structural thermal storage in residential buildings. Appl Energy 2017;198(15):192–202.
[8] Lund PD, Lindgren J, Mikkola J, Salpakari J. Review of energy system flexibility measures to enable high levels of variable renewable electricity. Renew Sustain Energy Rev 2015;45:785–807.
[9] Ruusu R, Cao S, Delgado BM, Hasan A. Direct quantification of multiple-source energy flexibility in a residential building using a new model predictive high-level controller. Energy Convers Manag 2019;180:1109–28.
[10] Clauß J, Stinner S, Sartori I, Georges L. Predictive rule-based control to activate the energy flexibility of Norwegian residential buildings: Case of an air-source heat pump and direct electric heating. Appl Energy 2019;237:500–18.
[11] Kazmi H, Suykens J, Balint A, Driesen J. Multi-agent reinforcement learning for modeling and control of thermostatically controlled loads. Appl Energy 2019;238:1022–35.
[12] Finck C, Li R, Zeiler W. Economic model predictive control for demand flexibility of a residential building. Energy 2019;176:365–79.
[13] Foteinaki K, Li R, Péan T, Rode C, Salom J. Evaluation of energy flexibility of low-energy residential buildings connected to district heating. Energy Build 2020. https://doi.org/10.1016/j.enbuild.2020.109804.
[14] Li Y, Wang C, Li G, Wang J, Zhao D. Chen C. Improving operational flexibility of integrated energy system with uncertain renewable generations considering thermal inertia of buildings Energy Conversion and Management 2020. DOI: 10.1016/j.enconman.2020.112526.
[15] Ramos JS, Moreno MP, Rodríguez LR, Delgado MG, Domínguez SA. Potential for exploiting the synergies between buildings through DSM approaches. Case study: La Graciosa Island. Energy Convers Manage 2019;194(15):199–216.
[16] Jensen SØ, Marszal-Pomianowska A, Lollini R, Pasut W, Knotzer A, Engelmann P, et al. IEA EBC Annex 67 Energy Flexible Buildings. Energy Build 2017;155:25–34.
[17] Huang Z, Xie Z, Zhang C, Chan SH, Milewski J, Xie Y, et al. Modeling and multi-objective optimization of a stand-alone PV-hydrogen-retired EV battery hybrid energy system. Energy Convers Manage 2019;181:80–92.
[18] Buonomano A. Building to Vehicle to Building concept: A comprehensive parametric and sensitivity analysis for decision making aims. Appl Energy 2020. https://doi.org/10.1016/j.apenergy.2019.114077.
[19] Cusenza MA, Guarino F, Longo S, Mistretta M, Cellura M. Reuse of electric vehicle batteries in buildings: An integrated load match analysis and life cycle assessment approach. Energy Build 2019;186:339–54.
[20] Rehman H, Reda F, Paiho S, Hasan A. Towards positive energy communities at high latitudes. Energy Convers Manage 2019;196(15):175–95.
[21] Quddus MA, Shahvari O, Marufuzzaman M, Usher JM, Jaradat R. A collaborative energy sharing optimization model among electric vehicle charging stations, commercial buildings, and power grid. Appl Energy 2018;229:841–57.
[22] Cao S. The impact of electric vehicles and mobile boundary expansions on the realization of zero-emission office buildings. Appl Energy 2019. https://doi.org/10.1016/j.apenergy.2019.113347.
[23] Flores RJ, Shaffer BP, Brouwer J. Electricity costs for a Level 3 electric vehicle fueling station integrated with a building. Appl Energy 2017;191:367–84.
[24] Barone G, Buonomano A, Calise F, Forzano C, Palombo A. Building to vehicle to building concept toward a novel zero energy paradigm: Modelling and case studies. Renew Sustain Energy Rev 2019;101:625–48.
[25] Zhou Y, Cao S, Hensen JLM, Lund PD. Energy integration and interaction between buildings and vehicles: A state-of-the-art review. Renew Sustain Energy Rev 2019. https://doi.org/10.1016/j.rser.2019.109337.
[26] Tang X, Wang Y, Zou C, Yao K, Xia Y, Gao F. A novel framework for Lithium-ion battery modeling considering uncertainties of temperature and aging. Energy Convers Manage 2019;180:162–70.
[27] Ahmadian A, Sedghi M, Elkamel A, Fowler M, Golkar MA. Plug-in electric vehicle batteries degradation modeling for smart grid studies: Review, assessment and conceptual framework. Renew Sustain Energy Rev 2018;81:2609–24.
[28] Yang R, Xiong R, He H, Mu H, Wang C. A novel method on estimating the degradation and state of charge of lithium-ion batteries used for electrical vehicles. Appl Energy 2017;207:336–45.
[29] Liu K, Hu X, Yang Z, Xie Y, Feng S. Lithium-ion battery charging management considering economic costs of electrical energy loss and battery degradation. Energy Convers Manage 2019;195:167–79.
[30] Thompson AW. Economic implications of lithium ion battery degradation for Vehicle-to-Grid (V2X) services. J Power Sources 2018;396:691–709.
[31] Uddin K, Gough R, Radcliffe J, Marco J, Jennings P. Techno-economic analysis of the viability of residential photovoltaic systems using lithium-ion batteries for energy storage in the United Kingdom. Appl Energy 2017;206:12–21.
[32] Salpakari J, Rasku T, Lindgren J, Lund PD. Flexibility of electric vehicles and space heating in net zero energy houses: an optimal control model with thermal dynamics and battery degradation. Appl Energy 2017;190:800–12.
[33] Mehrjerdi H, Iqbal A, Rakhshani E, Torres JR. Daily-seasonal operation in net-zero energy building powered by hybrid renewable energies and hydrogen storage systems. Energy Convers Manage 2019. https://doi.org/10.1016/j.enconman.2019.112156.
[34] Akhtari MR, Baneshi M. Techno-economic assessment and optimization of a hybrid renewable co-supply of electricity, heat and hydrogen system to enhance performance by recovering excess electricity for a large energy consumer. Energy Convers Manage 2019;188:131–41.
[35] Assunção A, Moura PS, Almeida AT. Technical and economic assessment of the secondary use of repurposed electric vehicle batteries in the residential sector to support solar energy. Appl Energy 2016;181:120–31.
[36] Yang Y, Bremner S, Menictas C, Kay M. Battery energy storage system size determination in renewable energy systems: A review. Renew Sustain Energy Rev 2018;91:109–25.
[37] Zhou Y, Cao S. Energy flexibility investigation of advanced grid-responsive energy control strategies with the static battery and electric vehicles: A case study of a high-rise office building in Hong Kong. Energy Convers Manage 2019. https://doi.org/10.1016/j.enconman.2019.111888.
[38] Meteonorm\Weather\Meteonorm\Asia\HK-Hong-Kong-Observatory-450050.tm2.
[39] Air-Cooled Liquid Chillers with Integrated Hydronic Module, 30RB 162-802 Nominal cooling capacity 162-774 kW. Available from https://climamarket.bg/wp-content/uploads/Tech-Spec-Carrier-30RB-162-802.pdf.
[40] Air-Cooled Liquid Chillers 10 to 60 Tons. CGAD090. https://mafiadoc.com/air-cooled-liquid-chillers-1060-tons-trane_59f355401723dd90e0ca20dc.html.
[41] Performance based building energy code 2007. Available from: https://www.emsd.gov.hk/filemanager/en/content_725/PBBEC_Guidelines_2007.pdf.
[42] SEL (Solar Energy Laboratory, Univ. of Wisconsin-Madison), TRANSSOLAR (TRANSSOLAR Energietechnik GmbH), CSTB (Centre Scientifique et Technique du Bâtiment), and TESS (Thermal Energy Systems Specialists). “TESSLibs 17 Component Libiaries for the TRNSYS Simulation Environment. Volume 06 HVAC Library Mathematical Reference,” the documentations attached in the software package of TRNSYS 18 for the TESS Models.
[43] SEL (Solar Energy Laboratory, Univ. of Wisconsin-Madison), TRANSSOLAR (TRANSSOLAR Energietechnik GmbH), CSTB (Centre Scientifique et Technique du Bâtiment), TESS (Thermal Energy Systems Specialists). “TESSLibs 17 Component libraries for the TRNSYS Simulation Environment, Volume 11 Storage tank Library Mathematical Reference.”.
[44] NISSAN LEAF Specs. Available from < http://www.mynissanleaf.com/wiki/images/0/06/NISSAN_LEAF_SpecSheet_FINAL_US_2.pdf > .
[45] Land Transport Guru. Available from < https://landtransportguru.net/st-autobus > .
[46] SEL (Solar Energy Laboratory, Univ. of Wisconsin-Madison), TRANSSOLAR (TRANSSOLAR Energietechnik GmbH), CSTB (Centre Scientifique et Technique du Bâtiment), TESS (Thermal Energy Systems Specialists). “TRNSYS 18 A TESSLibs 17 Volume 03 Electrical Library, Mathematical Reference,” the documentations attached in the software package of TRNSYS 18 for the TESS Component Library.
[47] SEL (Solar Energy Laboratory, Univ. of Wisconsin-Madison), TRANSSOLAR (TRANSSOLAR Energietechnik GmbH), CSTB (Centre Scientifique et Technique du Bâtiment), “TRNSYS 18 Volume 04, Mathematical Reference,” the documentations attached in the software package of TRNSYS 18.
[48] ATB Riva Calzoni ATB 500 kW. https://en.wind-turbine-models.com/turbines/1533-atb-riva-calzoni-atb-500.54.
[49] Bulk Tariff. https://www.clp.com.hk/en/customer-service/tariff/business-and-other-customers/bulk-tariff; 2018.
[50] Zhou Y, Cao S, R Kosonen, M Hamdy. Multi-objective optimisation of an interactive buildings-vehicles energy sharing network with high energy flexibility using the Pareto archive NSGA-II algorithm. Energy conversion and management 2019. Under review.
[51] RA12-200D. https://docs-emea.rs-online.com/webdocs/0ceb/0900766b80ceb2db.pdf.
[52] AGM battery. https://www.racshop.co.uk/advice/what-is-an-agm-battery.
[53] Severson KA, Attia PM, Jin N, Perkins N, Jiang B, Yang Z, et al. Data-driven prediction of battery cycle life before capacity degradation. Nat Energy 2019. https://doi.org/10.1038/s41560-019-0356-8.
[54] HKCEF. Guidelines to Account for and Report on Greenhouse Gas Emissions and Removals for Buildings (Commercial, Residential or Institutional Purposes) in Hong Kong.https://www.epd.gov.hk/epd/english/climate_change/files/CAGuidelines_Eng.pdf; 2010.
[55] Ogunjuyigbe ASO, Ayodele TR, Akinola OA. Optimal allocation and sizing of PV/Wind/Split-diesel/Battery hybrid energy system for minimizing life cycle cost, carbon emission and dump energy of remote residential building. Appl Energy 2016;171:153–71.
[56] Tumminia G, Guarino F, Longo S, Aloisio D, Cellura S, Sergi F, et al. Grid interaction and environmental impact of a net zero energy building. Energy Convers Manage 2020. https://doi.org/10.1016/j.enconman.2019.112228.
[57] Delgado BM, Cao S, Hasan A, Sirén K. Multiobjective optimization for lifecycle cost, carbon dioxide emissions and exergy of residential heat and electricity prosumers. Energy Convers Manage 2017;154:455–69.
[58] Roberts MB, Bruce A, Gill IM. Impact of shared battery energy storage systems on photovoltaic self-consumption and electricity bills in apartment buildings. Appl

Energy 2019;245:78–95.
[59] Litjens GBMA, Worrell E, Sark WGJHM. Lowering greenhouse gas emissions in the built environment by combining ground source heat pumps, photovoltaics and battery storage. Energy Build 2018;180:51–71.
[60] Murray P, Marquant J, Niffeler M, Mavromatidis G, Orehounig K. Optimal transformation strategies for buildings, neighbourhoods and districts to reach CO2 emission reduction targets. Energy Build 2020. https://doi.org/10.1016/j.enbuild.2019.109569.
[61] Zhou Y, Cao S. Quantification of energy flexibility of residential net-zero-energy buildings involved with dynamic operations of hybrid energy storages and diversified energy conversion strategies Sustainable Energy. Grids Networks 2020. https://doi.org/10.1016/j.segan.2020.100304.
[62] Akter MN, Mahmud MA, Amanullah MTO. Comprehensive economic evaluations of a residential building with solar photovoltaic and battery energy storage systems: An Australian case study. Energy and Buildings 201; 138: 332-46.
[63] Aelenei D, Lopes RA, Aelenei L, Gonçalves H. Investigating the potential for energy flexibility in an office building with a vertical BIPV and a PV roof system. Renewable Energy 2019;137:189–97.
[64] Phan QA, Scully T, Breen M, Murphy MD. Determination of optimal battery utilization to minimize operating costs for a grid-connected building with renewable energy sources. Energy Convers Manage 2018;174:157–74.
[65] Liu K, Li K, Ma H, Zhang J, Peng Q. Multi-objective optimization of charging patterns for lithium-ion battery management. Energy Convers Manage 2018;1591:151–62.
[66] Pelzer D, Ciechanowicz D, Aydt H, Knoll A. A price-responsive dispatching strategy for Vehicle-to-Grid: An economic evaluation applied to the case of Singapore. J Power Sources 2014;256:345–53.
[67] Khatib T, Ibrahim IA, Mohamed A. A review on sizing methodologies of photovoltaic array and storage battery in a standalone photovoltaic system. Energy Convers Manage 2016;120:430–48.